EUMETSAT

ROM SAF

RADIO OCCULTATION METEOROLOGY

ROM SAF CDOP-3

Visiting Scientist Report 40:

Analysis of decadal trends from RO as contributed to IPCC AR6

Florian Ladstädter

ROM SAF Consortium
Danish Meteorological Institute (DMI)
European Centre for Medium-Range Weather Forecasts (ECMWF)
Institut d'Estudis Espacials de Catalunya (IEEC)
Met Office (UKMO)

Ref: SAF/ROM/DMI/REP/VS/40
Version: 1.0
Date: 16 August 2021

DOCUMENT AUTHOR TABLE

	Author(s)	*Function*	*Date*
Prepared by:	F. Ladstädter	ROM SAF Visiting Scientist	16/8 2021
Reviewed by (Internal):	H. Gleisner	ROM SAF Climate Coordinator	1/6 2021
Reviewed by (Internal):	S. B. Healy	ROM SAF Science Coordinator	24/6 2021
Approved by:	S. B. Healy	ROM SAF Science Coordinator	8/7 2021
Approved by:	K. B. Lauritsen	ROM SAF Project Manager	16/8 2021

DOCUMENT CHANGE RECORD

Version	*Date*	*By*	*Description*
Version 0.1	31/5 2021	FL	Draft version
Version 0.9	7/7 2021	FL	Updated version after review
Version 1.0	16/8 2021	FL	Final version

DOCUMENT DISTRIBUTION LIST

This VS report is made available at the ROM SAF website.

VS AUTHOR AND DURATION

VS Authors

This visiting scientist report was prepared by Dr. Florian Ladstädter, Senior Scientist at Wegener Center for Climate and Global Change, Univ. of Graz, Austria;
Email: florian.ladstaedter@uni-graz.at.

VS Duration

The VS study was performed during October 2020 to May 2021 at the Wegener Center, Univ. of Graz, Austria.

ROM SAF

The Radio Occultation Meteorology Satellite Application Facility (ROM SAF) is a decentralised processing centre under EUMETSAT which is responsible for operational processing of radio occultation (RO) data from the Metop and Metop-SG satellites and radio occultation data from other missions. The ROM SAF delivers bending angle, refractivity, temperature, pressure, humidity, and other geophysical variables in near real-time for NWP users, as well as reprocessed Climate Data Records (CDRs) and Interim Climate Data Records (ICDRs) for users requiring a higher degree of homogeneity of the RO data sets. The CDRs and ICDRs are further processed into globally gridded monthly-mean data for use in climate monitoring and climate science applications.

The ROM SAF also maintains the Radio Occultation Processing Package (ROPP) which contains software modules that aid users wishing to process, quality-control and assimilate radio occultation data from any radio occultation mission into NWP and other models.

The ROM SAF Leading Entity is the Danish Meteorological Institute (DMI), with Cooperating Entities: i) European Centre for Medium-Range Weather Forecasts (ECMWF) in Reading, United Kingdom, ii) Institut D'Estudis Espacials de Catalunya (IEEC) in Barcelona, Spain, and iii) Met Office in Exeter, United Kingdom. To get access to our products or to read more about the ROM SAF please go to: http://www.romsaf.org.

Intellectual Property Rights

List of Contents

Executive Summary

The timeline of Radio Occultation (RO) measurements has now become sufficiently long to be used for one of its promising applications, which is climatological trend detection. This has also been recognized by the Intergovernmental Panel on Climate Change (IPCC), which invited the RO community to submit a contribution about upper-air temperature changes to the sixth assessment report (AR6). The present visiting scientist report summarizes and extends the work which has been performed in the course of this contribution to the IPCC, also building on previous work.

While, in general, the properties of the RO technique are favorable for the high-accuracy requirements of (short-term) trend detection, there are still open questions related to the impacts of various RO specifics on trend estimates. A detailed knowledge about sources of trend uncertainty is therefore required. This report addresses some of the potential factors influencing the trend estimates.

It is shown that biases between CHAMP, F3C, and Metop are of relevance for the trend estimates, especially for parameters at the end of the retrieval chain and at higher altitudes.

The impact of the vertical coordinate used to compute and present trends needs to be taken into account, especially when comparing to other datasets having pressure as their native vertical coordinate. This impact due to the rising levels of constant pressure with global warming is quantified, and shown to be relevant.

The influence of the reference field used for Sampling Error (SE) correction is discussed, and shown to have non-negligible impact on the fine structure of the trend estimates. This is a result of the CHAMP period having a significantly lower number of measurements than later periods. The impact of the limited local time coverage of Metop, and its compensation by the SE correction is also addressed as another possible impact.

Finally, general aspects of computing trend estimates and their significance from shorter time series in the presence of comparatively strong natural variability are discussed.

1 Introduction

Due to its long-term stability, high vertical resolution, and global coverage Radio Occultation (RO) is considered to be very valuable for upper-air trend analysis. The rather short available time series has hindered efforts to determine quantitative trend estimates in the past. A careful consideration of natural variability and sources of trend uncertainty is needed. Work on determining these uncertainties and on RO trend analysis has been conducted by several research centers in the past [e.g. 8, 3, 9].

A consolidated effort on RO trend analysis was triggered with the invitation to submit an upper-air temperature contribution to Working Group 1 of the sixth Intergovernmental Panel on Climate Change (IPCC) Assessment Report (IPCC AR6)[1] [4] in March 2019. The work was coordinated by Axel von Engeln at European Organization for the Exploitation of Meteorological Satellites (EUMETSAT), and included researchers from EUMETSAT, Radio Occultation Meteorology Satellite Application Facility (ROM SAF), Wegener Center for Climate and Global Change (WEGC), National Oceanic and Atmospheric Administration (NOAA), University Corporation for Atmospheric Research (UCAR), Jet Propulsion Laboratory (JPL), German Research Centre for Geosciences (GFZ), Met Office, and European Centre for Medium-Range Weather Forecasts (ECMWF). Existing data sets were quickly compiled at the involved centers, trends were calculated, preliminary graphics were generated, and a first draft of the RO contribution ("First order draft", FOD) was agreed upon and submitted to the IPCC on March 28, 2019. The RO contribution included two parts: (a) globally averaged (85S–85N) monthly mean Microwave Sounding Unit (MSU)/Advanced MSU (AMSU) temperature anomaly data for the Upper Troposphere–Lower Stratosphere (UTLS) region and equivalent radiosonde and RO data, and (b) RO-based dry temperature trends in the 20S–20N and 70S–70N latitude regions over the 16-year time period 2002 to 2018. The latter RO-based trend data were also shown as latitudinally resolved zonal plots.

After additional work during the autumn of 2019, related to understanding differences among the RO processing centers, handling of different type of vertical coordinates, comparisons with other observation types (Atmospheric Infrared Sounder (AIRS), radiosondes), discussing the proper methods for quantifying errors, etc., the first draft was updated with new graphics (similar to Figure 1.1 and others) and relevant text changes. On December 19, 2019, that updated version ("Second order draft", SOD) was submitted to the IPCC.

During the work with the RO time series and trends for the IPCC AR6 contribution, several questions related to choices in the climatological RO data processing and trend calculations were addressed. That included the binning methods, Sampling Errors (SEs) and correction of sampling errors, impacts of included satellite missions, and the quality of the computed trends. In addition to trends in dry temperature anomaly data, trends in refractivity and bending angle (i.e., the physical variables from which dry temperatures are derived) were also briefly investigated. Most of this additional work was done by a small team from the ROM SAF and the WEGC.

This visiting scientist project aims at consolidating the work on RO trend analysis, addressing some of these outstanding questions that were only briefly touched upon during the work with the IPCC AR6 contribution.

[1] See https://www.ipcc.ch/report/ar6/wg1/

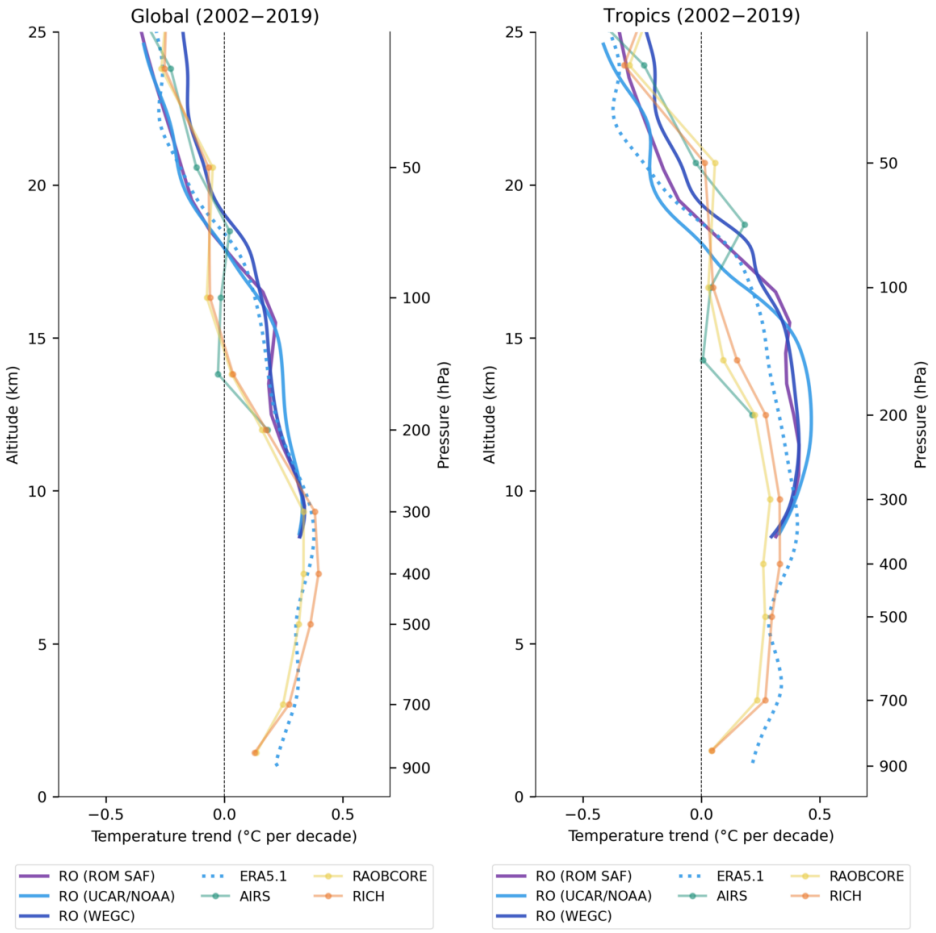

Figure 1.1: *Decadal temperature trends from several radio occultation and radiosonde datasets, as well as from AIRS data, for near-global means (left) and tropics (right). A similar figure appears in the IPCC AR6 Working Group 1 report, see* https://www.ipcc.ch/report/ar6/wg1/.

2 The impact of included satellite missions

RO measurements have beneficial properties for climate studies, and thus for trend analysis. Among those, the traceability of the measurement to the SI unit of the second is particularly useful. With that, the creation of a seamless time series without the need of intercalibration between missions is, in principle, possible [1, 2].

However, subtle differences between RO missions and instruments can possibly influence the retrieval of geophysical parameters and propagate to the monthly mean data used in climate studies [3].

This chapter aims to roughly estimate the quantitative impact of those differences on climatological trends. For a more detailed analysis on the underlying causes of those differences see [e.g., 3, 8, 1, 6].

2.1 Sensitivity of the trend on the involved missions

In this section, the sensitivity of the trend values on the specifics of the involved missions are analyzed using both single-satellite and combined time series for several missions, and using data from WEGC and ROM SAF.

The following datasets are inter-compared:

Dataset	Missions
WEGC RO (all sats)	CHAMP, F3C, GRACE, Metop
WEGC RO (single sats)	CHAMP, F3C FM1 (starting 2008-10; some FM6 filling gaps), Metop-A (after 2018-06)
WEGC RO (COSMIC)	All F3C sats
WEGC RO (Metop-A)	Metop-A
ROM SAF RO (all sats)	CHAMP, F3C (until 2016-12), GRACE (until 2016-12), Metop
ROM SAF RO (Metop-A)	Metop-A
ROM SAF RO (F3C)	F3C (until 2016-12)

Temperature trends for tropics and near-global for these datasets are shown in Figure 2.1 to Figure 2.3. In these plots, the left panel shows tropics, and the right panel shows near-global. These are all SE-corrected. The actual trend values are not relevant due to the short time period. The time period is chosen to provide the maximum common time span for all datasets. Challenging Mini-Satellite Payload (CHAMP) only contributes in the first few months, ending in 2008-09.

There are a couple of interesting features in Figure 2.1. Meteorological Operational-A (Metop-A) trends start to deviate above the tropopause/around 22 km in the tropics. ROM SAF and WEGC Metop-A trends are very close up to at least 30 km, and down to about 16 km. Below that there seem to be a problem with WEGC Metop-A trends, with a large deviation to all other datasets. Around the tropical tropopause, two groups of datasets with a difference in trends of around 0.1 K can be distinguished: Metop-A for ROM SAF and WEGC,

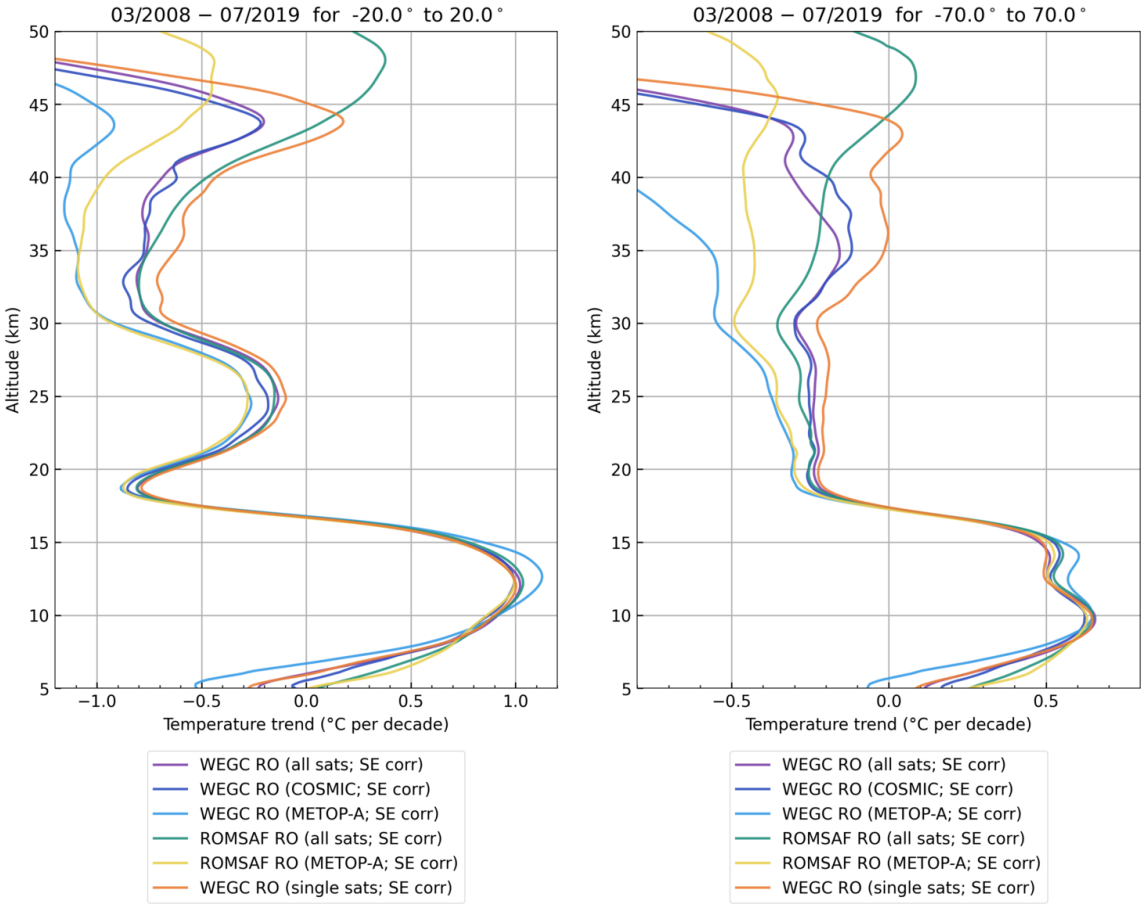

Figure 2.1: *Impact of including different RO missions for a common time span of 2008-03 to 2019-07. Shown are dry temperature trends, (left) tropics, (right) near-global.*

and WEGC FORMOSAT-3/COSMIC (F3C) have slightly smaller trends than the "all sats" datasets of both centers. Also the "single sats" dataset of WEGC belongs to this group– maybe showing the influence of CHAMP in the first couple of months. WEGC F3C slowly changes its behavior from being close to Metop-A below around 22 km, and coming closer to the "all sats" datasets of both WEGC and ROM SAF. It is interesting to see that also ROM SAF, which shows less impact of high-altitude initialization than WEGC, has different trend values for Metop-A and "all sats". This is also clearly visible in the "near-global" plot (Figure 2.1 right panel).

It is interesting to see that WEGC temperature trends for "all-sats" are dominated by F3C, and Metop-A deviates quite strongly from those values. This is also the case for ROM SAF. A closer look on the difference between ROM SAF Metop-A and F3C can be found in Figure 2.2, which is a separate figure since it contains a shorter common time range of 2008-03 to 2016-12, due to ROM SAF only providing F3C data up to this date. Again Metop-A stands out compared to F3C or "all-sats" trends.

See [3] for an analyses of biases between trends from Meteorological Operational (Metop), F3C, and multi-satellite datasets.

To rule out possible effects of the SE correction, Figure 2.3 shows that the impact of the SE

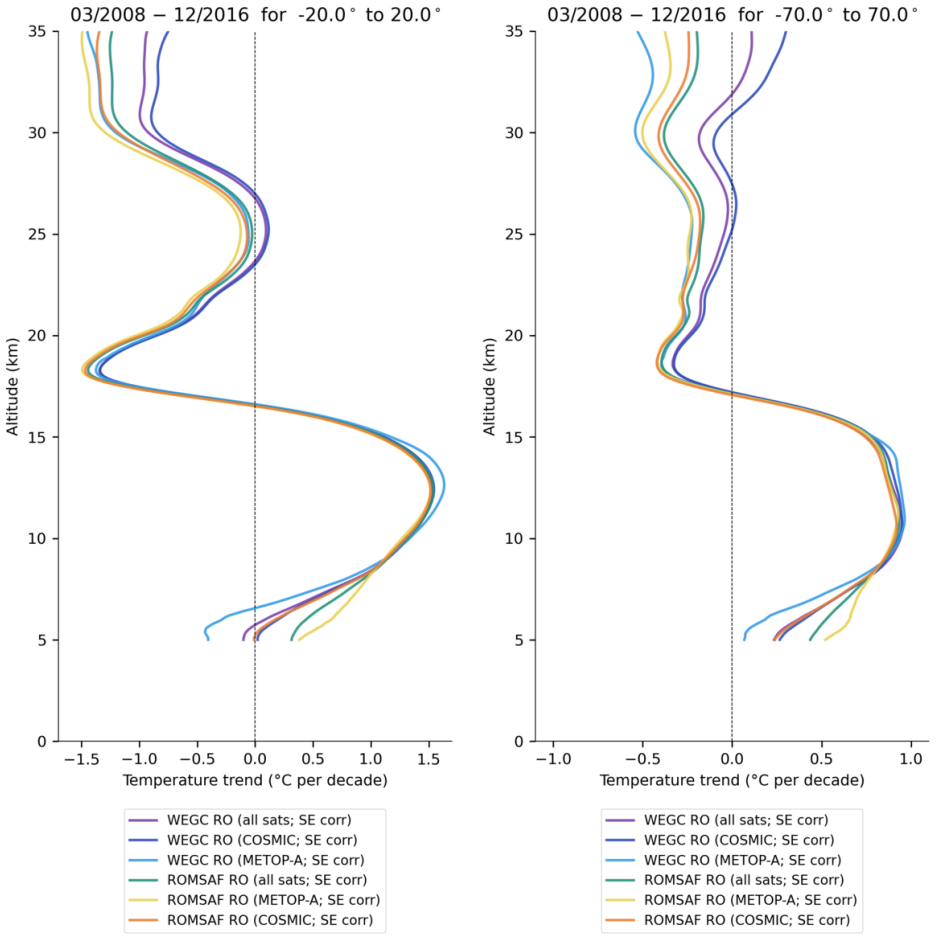

Figure 2.2: *Impact of including different RO missions for a shorter common time span of 2008-03 to 2016-12 to also accommodate F3C-only for ROM SAF.*

correction is, as expected, rather small for these missions.

Next, the chain of RO variables is examined.

For refractivity (Figure 2.4) trends, the behavior is similar to temperature with the difference that F3C trends are following the Metop-A trends up to about 30 km to 35 km, and starts to deviate only above that.

For non-optimized (Figure 2.5) and optimized (Figure 2.6) bending angle trends, it is interesting to see that the non-optimized bending angle trends are very similar for all WEGC datasets, with the exception of Metop-A in the range of 10 km to 17 km (an indication that this is a bug in the WEGC retrieval). After optimization, the influence of the high-altitude initialization becomes visible in the bending angle trends above about 30 km, where F3C and Metop-A are increasingly separated from the "all sats" and "single sats" datasets; possibly an effect of CHAMP.

2.2 Bias between CHAMP and F3C

To investigate biases between CHAMP and other missions, one option is to use co-located profiles of CHAMP and F3C, which have an overlapping time range from 2006-08 to 2008-

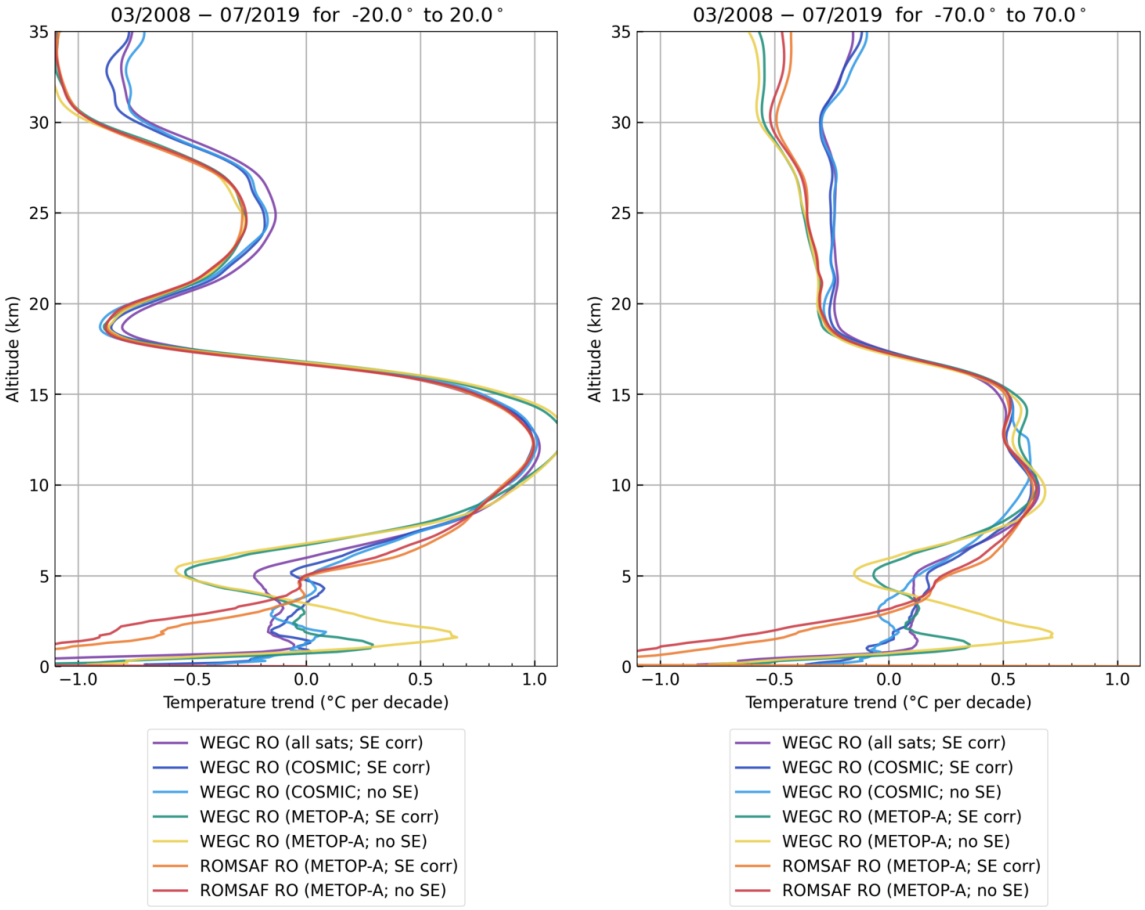

Figure 2.3: *Impact of including different RO missions and the corresponding sampling-error correction for a common time span of 2008-03 to 2019-07. Shown are dry temperature trends.*

10.

In the following, all pairs of CHAMP and F3C profiles which fulfill the matching criteria of a spatial distance of less than 100 km and a temporal difference of less than 1 h are considered. Shown are differences of CHAMP minus F3C.

In Figure 2.7, the mean dry temperature differences of CHAMP minus F3C for the time range 2006-09 to 2008-09 are shown for various latitude ranges. RO data from WEGC (OPSv56), ROM SAF, and UCAR are included. The global bias up to an altitude of about 20 km between CHAMP minus F3C is less than −0.1 K for WEGC, and even less (but positive) for ROM SAF and UCAR. Above about 20 km, the bias increases to −0.2 K for WEGC, and 0.2 K to 0.4 K for ROM SAF and UCAR.

A slightly better latitudinal resolution is shown in Figure 2.8, with the same data presented as a contour plot based on 30° latitudinal bands.

In summary, CHAMP dry temperature is more negative compared to F3C for WEGC data, and more positive for ROM SAF and UCAR above about 10 km (for WEGC), and increasingly above 20 km (for all three centers). This certainly contributes to differences in trend estimates between these centers.

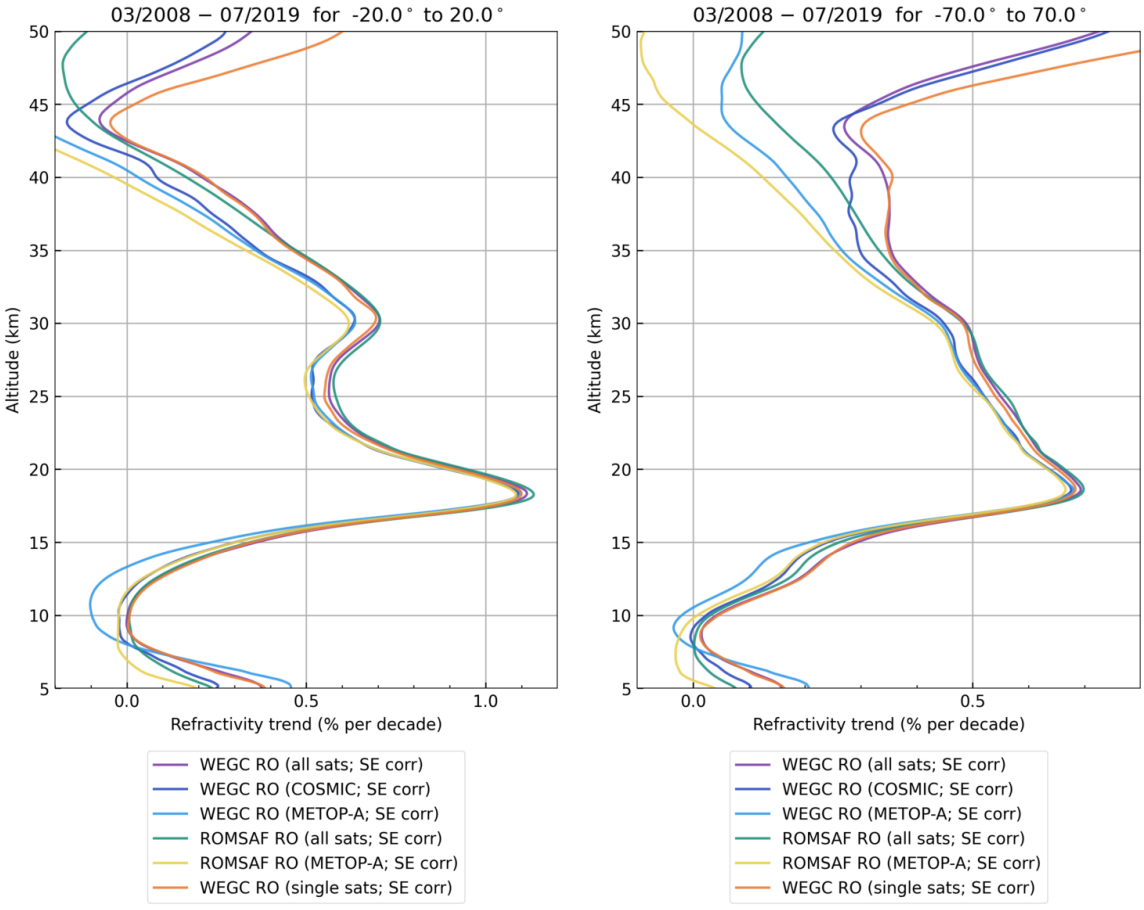

Figure 2.4: *Impact of including different RO missions for refractivity trends, for a common time span of 2008-03 to 2019-07.*

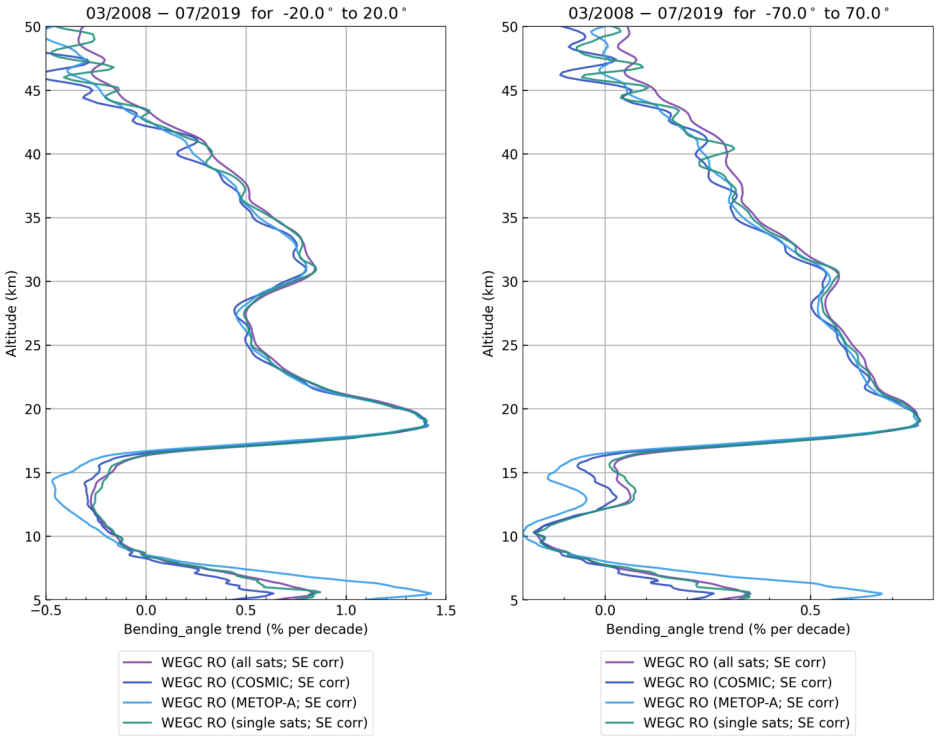

Figure 2.5: *Impact of including different RO missions for non-optimized bending angle trends, for a common time span of 2008-03 to 2019-07.*

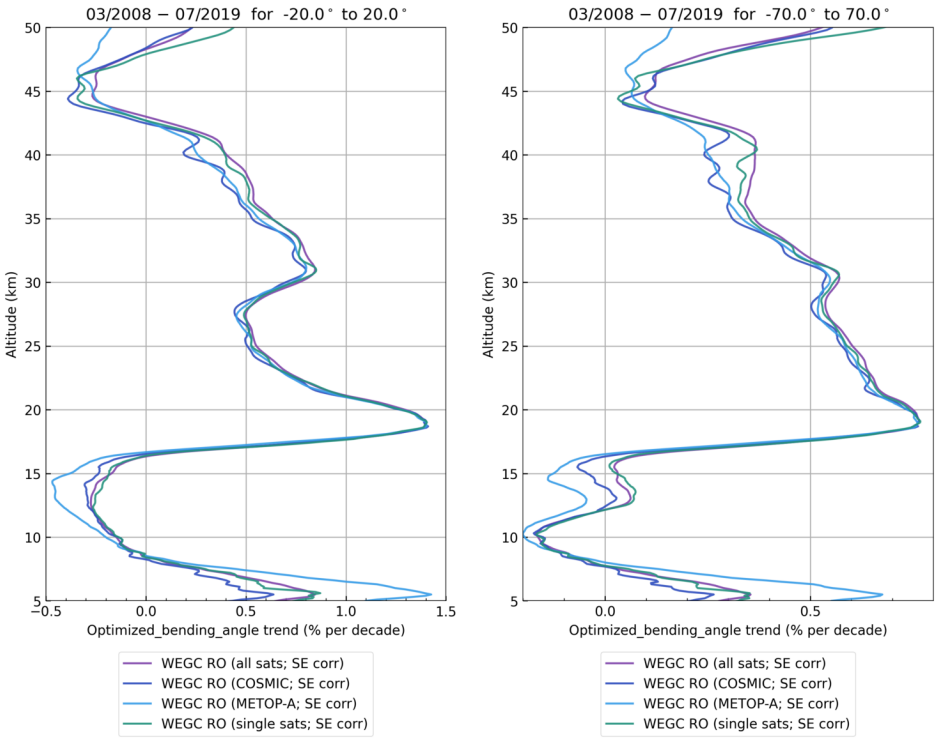

Figure 2.6: *Impact of including different RO missions for optimized bending angle trends, for a common time span of 2008-03 to 2019-07.*

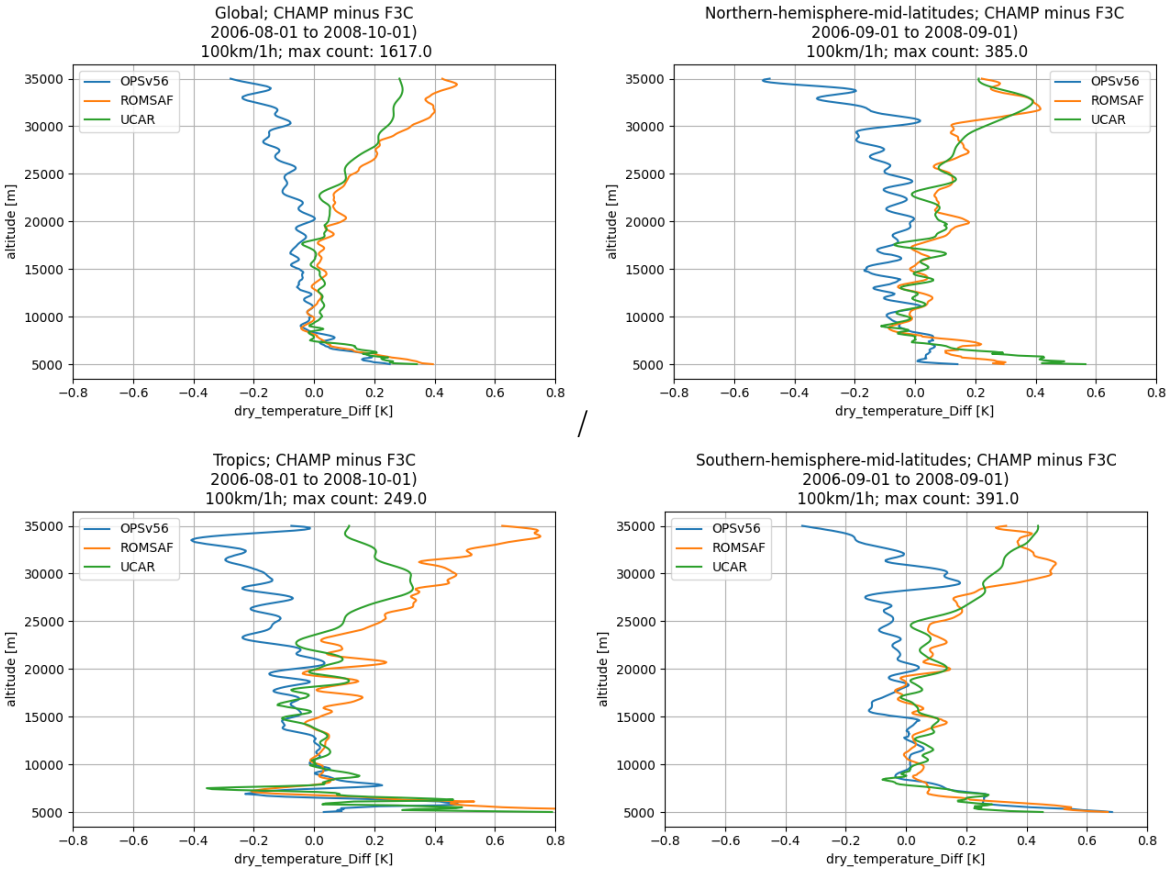

Figure 2.7: *CHAMP minus F3C for specific latitude ranges, for the time range 2006-09 to 2008-09. Shown are RO dry temperature data from WEGC (OPSv56), ROMSAF, and UCAR. (left top) global; (right top) Northern mid-latitudes,* 20°*N to* 60°*N; (left bottom) tropics,* 20°*S to* 20°*N; (right bottom) Southern mid-latitudes,* 20°*S to* 60°*S.*

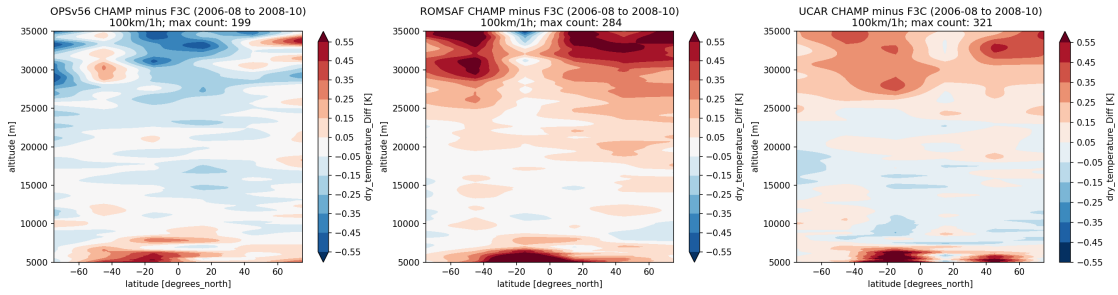

Figure 2.8: *CHAMP minus F3C for* 30° *latitude bands, for the time range 2006-09 to 2008-09. Shown are RO dry temperature data from WEGC (OPSv56; left), ROMSAF (center), and UCAR (right).*

3 The impact of the vertical coordinate

3.1 Profile-based processing on altitude or pressure

In the following, the influence of the chosen vertical coordinate on trend results is investigated. To this end, the same trend (e.g., temperature trend for a certain region over 2002 to 2019) is computed based on altitude or pressure coordinate.

The retrieved Radiosonde Observation (RAOB) data are originally already on a pressure grid, and are only interpolated (lin-log) to a fixed pressure grid for the shown "RS pres" data. This fixed pressure grid consists of 364 levels between 1000 hPa and 10 hPa, with approximately equal spacing in altitude space. The corresponding reference profiles (from ECMWF Re-Analysis Version 5.1 (ERA5.1)) have been converted from an altitude grid to pressure profile-wise (for each profile interpolated towards the location of the RAOB station).

For the altitude-based RAOB data (denoted as "RS" or "RS alt"), conversion to the altitude grid is performed as follows: For each RAOB profile (on its native pressure grid), the mapping from pressure to altitude is taken from its corresponding reference file (interpolated from ERA5.1 GRIB fields). Each RAOB profile is interpolated towards the pressure values of the reference profile, and then the coordinate is swapped from pressure to altitude.

The full "ERA5.1 pres" field is converted profile-wise (on its "native" 2.5x2.5 6-hourly space-time grid) from altitude to pressure.

The native coordinate for RO temperature data is altitude. For the pressure-based RO data ("RO pres"), the physical pressure of RO is taken profile-wise to switch the coordinate from altitude to pressure, and interpolate the resulting grid to a fixed pressure grid.

Figure 3.1 shows the impact in terms of temperature trends when using altitude or pressure as profile-wise coordinate for RO, RAOB, and ERA5.1. The plot coordinate is altitude, and the trends on pressure are converted to trends on altitude using the "empirical"[1] method.

Looking at Figure 3.1 it becomes evident that the trend based on the pressure coordinate is less positive up to about tropopause-height compared to the altitude-based trends. Above that the opposite is visible, the pressure-based trends are more positive than the altitude-based trends. This is consistent for all three datasets (RO, radiosonde, and ERA5.1 trends), which is an indicator that this behavior is not related to the different dataset characteristics and processings. Note again that RAOB is originally on a pressure grid, while RO and ERA5.1 are originally on altitude. RAOB and ERA5.1 are not independent of each other, since the conversion of the pressure-based RAOB to altitude-based RAOB is using ERA5.1 pressure-altitude mapping as outlined above. The SE correction of RO and RAOB is also computed using ERA5.1 data. The influence of the latter can be studied in Figure 3.2 (right panel). While the SE correction has a large influence on the trend values, the relative difference between pressure- and altitude-based data is similar for the non-SE corrected RAOB data and the corrected data.

Figure 3.2 shows radiosonde and ERA5.1 temperature trends over Europe for data computed on altitude and on pressure, with a similar behavior as shown before. The plot coordinate is

[1] The "empirical" method uses a mean mapping of pressure-to-altitude using several years of RO data for the specific latitude range shown.

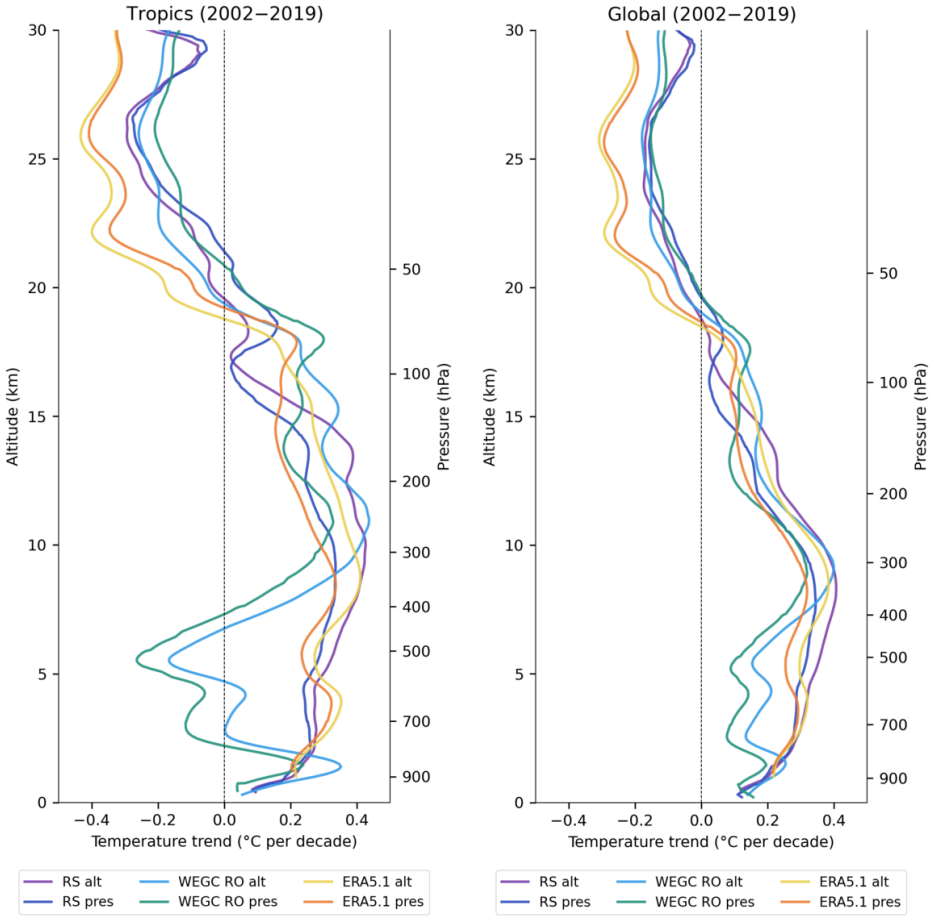

Figure 3.1: *Temperature trends for datasets computed profile-wise on altitude and on pressure grid, (left) tropics, (right) near-global.*

altitude.

This behavior of the temperature trend is consistent with an expected positive trend of the pressure on constant altitude levels, i.e. with the rising of levels of constant pressure with global warming: For regions of positive lapse rate (decreasing temperature, troposphere), a rising of constant pressure levels means that the same pressure level will be higher up, i.e. at lower temperatures. When determining temperature trends on constant pressure levels, this introduces a negative trend, superimposed on the overall positive temperature trend in the troposphere. For a negative lapse rate, i.e. in the stratosphere, the effect is reversed.

To get a quantitative estimate, we assume a pressure trend of about 0.2 % or 40 Pa/decade at 20000 Pa, see Figure 3.3. Using the simple pressure altitude formula

$$h = -7000 \ln(p/101325) \tag{3.1}$$

we get an estimate of the altitude difference related to this pressure trend as:

$$\Delta h = 7000 \ln(p_2/p_1) = 7000 \ln(20040/20000) \approx 14 \text{ m}. \tag{3.2}$$

With an approximate lapse rate of 7 K/km this corresponds to about $7/1000 \times 14 = 0.1$ K.

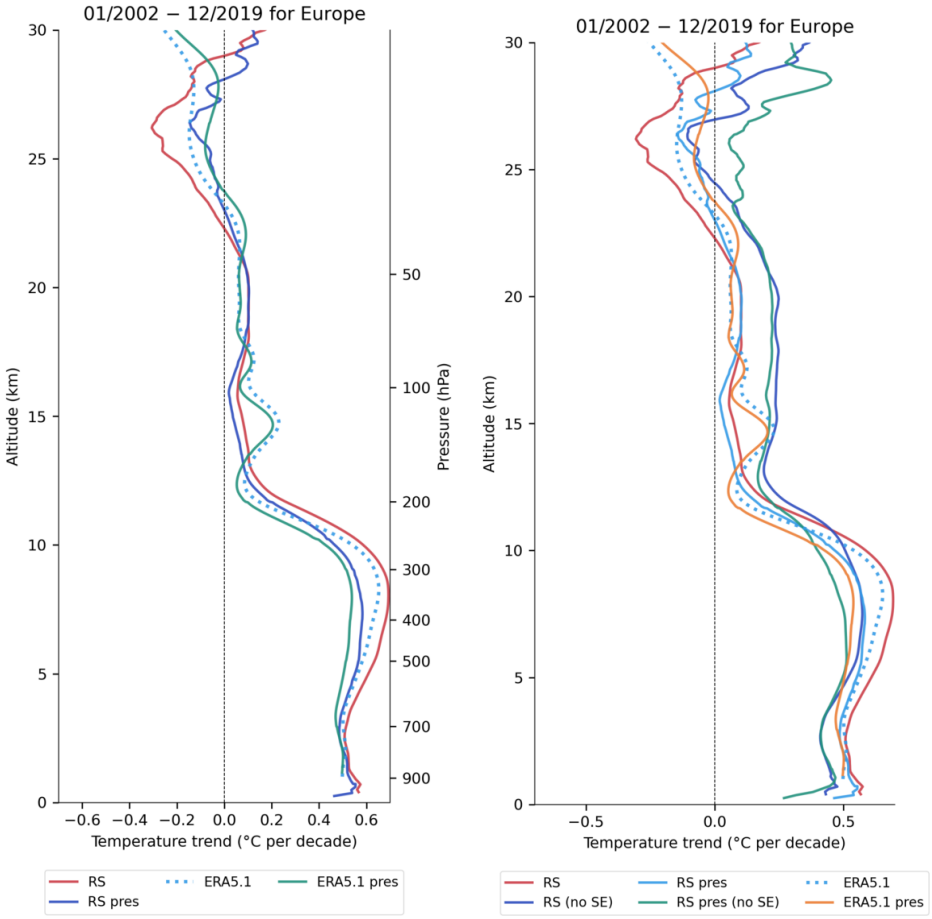

Figure 3.2: *Temperature trends over Europe for 2002 to 2019. The right panel also includes the impact of the SE correction.*

This value is in approximate agreement with the observed trend differences in Figure 3.1.

3.2 Impact of mapping trends from altitude to pressure grid

As shortly discussed above in section 3.1, to plot trends based on altitude coordinate together with trends on pressure coordinate, a mapping between altitude and pressure is needed.

The choices made for this mapping can influence the fine structure of the vertically resolved trends. To illustrate this, Figure 3.4 and Figure 3.5 show two different mapping methods. The "empirical" method uses a SE-corrected RO climatology of pressure on altitude levels over 2006 to 2015 in 10° bands. Aggregating these latitude bands to the latitude range according the data to plot (e.g., tropical or near-global) results in the "empirical" mapping between altitude and pressure.

The "simple" method uses the pressure altitude equation from Equation 3.1. This equation assumes zero lapse rate, as a result the trend on pressure coordinate, mapped to altitude, is shifted relative to the trend on altitude, especially in the troposphere. This shift can amount to more than 1 km.

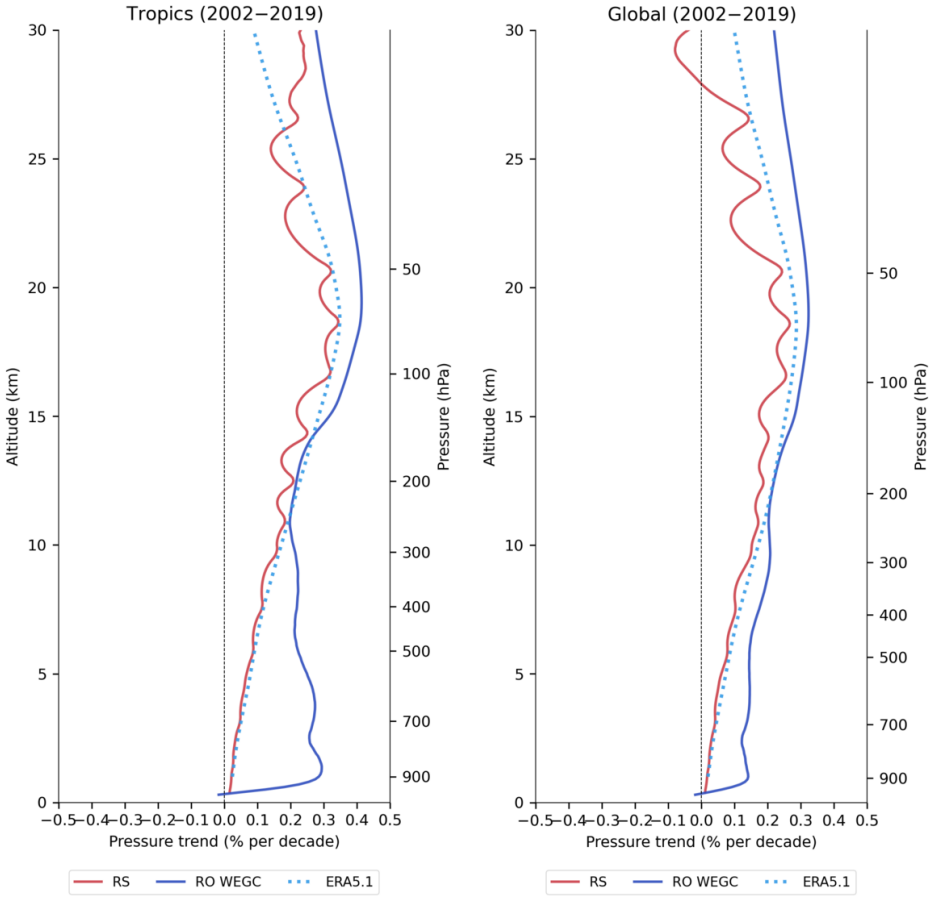

Figure 3.3: *Pressure trends, tropics (left), near-global (right).*

Comparing the two methods, “empirical” seems to be more adequate for this type of application.

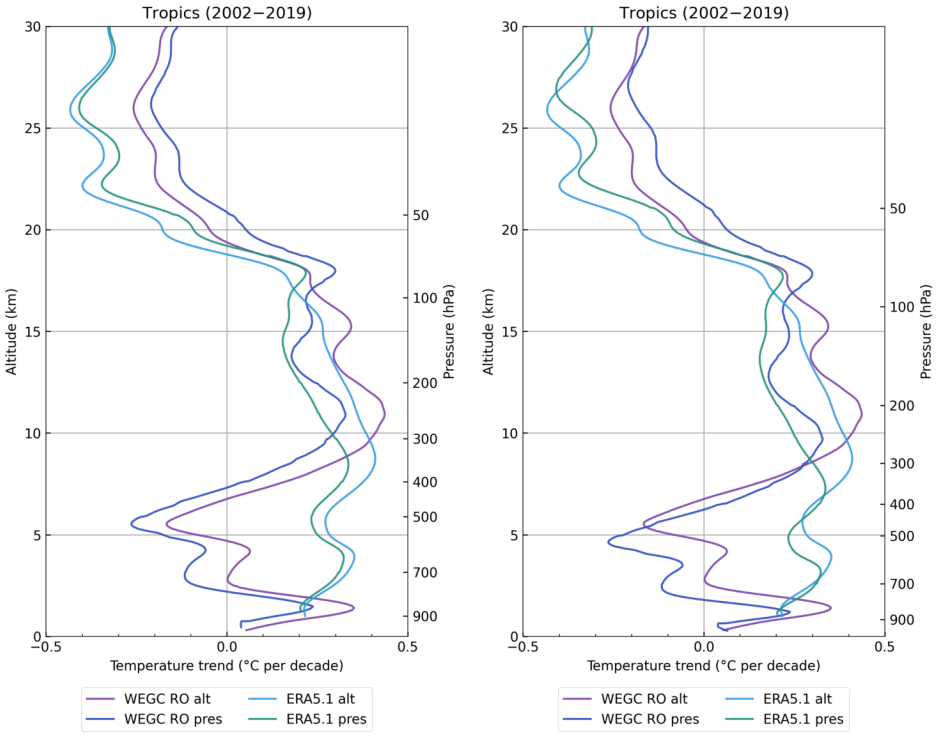

Figure 3.4: *Tropical temperature trends for altitude and pressure-based datasets. The vertical plot coordinate is altitude, for the pressure-based datasets a mapping to these altitude values is used. Mapping method: left: "empirical", right: "simple".*

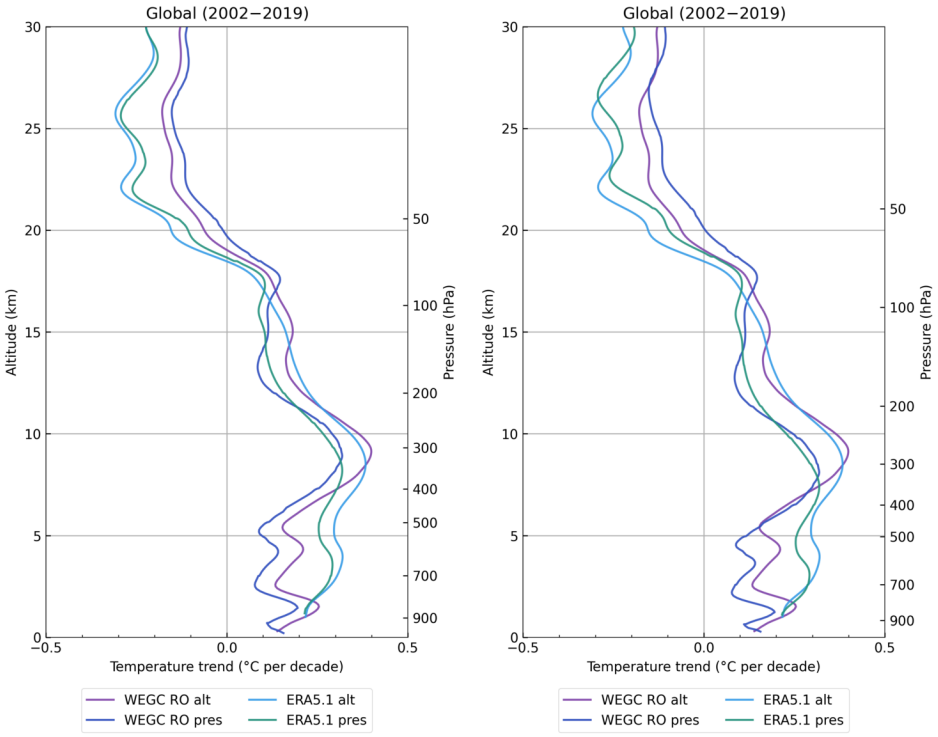

Figure 3.5: *Near-global temperature trends for altitude and pressure-based datasets. The vertical plot coordinate is altitude, for the pressure-based datasets a mapping to these altitude values is used. Mapping method: left: "empirical", right: "simple".*

4 The impact of the reference field on the SE

In this chapter the influence of the choice of reference field used for SE correction is investigated. In principle, the SE correction should be rather insensitive to the choice of reference field, since specific features of the model field should cancel out when subtracting the co-located reference field from the full reference field.

This approach only works if the data to be corrected have already an appropriate coverage of atmospheric variability. In the case of RO, the large change in coverage when the F3C mission enters the timeline makes a proper SE correction important to account for this change in the number of measurements. For missions on Sun-synchronous orbits (such as Metop), the bias due to an insufficient local-time coverage can be reduced, but for this, the reference field needs to correctly sample the diurnal and semi-diurnal cycle.

It is interesting to see that the SE corrected WEGC RO trends have a vertical wave-like structure, clearly coming from the SE correction. It seems that this is a feature of the reference fields (Figure 4.1).

To investigate the impact of the reference field on the trends further, Figure 4.2 (left panel) also includes trends computed from SE corrected time series which use a different reference field for the first and the second half of the time series. The dominant part here is the first half of the time series, including the CHAMP period. That means, the reference field chosen for the CHAMP period largely determines the influence of the sampling error correction on the fine structure of the trend.

Figure 4.2 (right panel) also includes ROM SAF RO data. The “external” ROM SAF trends were computed at ROM SAF, using mostly ECMWF Re-Analysis Interim (ERA-Interim) as reference field, whereas the “internal” ROM SAF trends were computed at WEGC, using ERA5.1 as reference. Apparently the differences between the RO retrieval methods, and possibly other differences between the RO datasets, dominate the trend characteristics. For the fine structure of the trends, the chosen reference field also plays an important role.

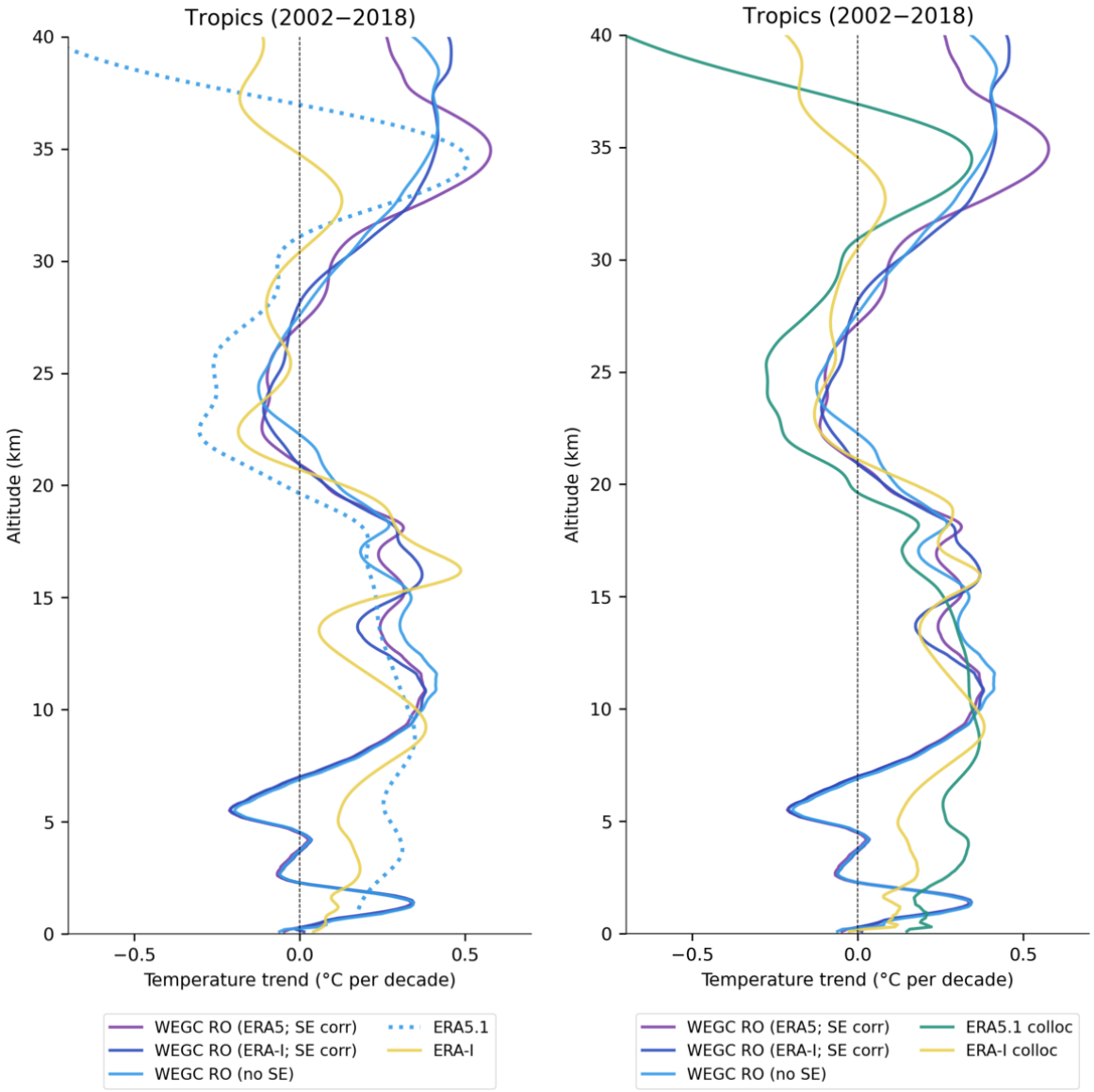

Figure 4.1: *Temperature trends from WEGC RO, without SE correction and corrected using ERA-Interim and ERA5.1. (Left) Compared to trends of the corresponding full field. (Right) Compared to the corresponding co-located reference field.*

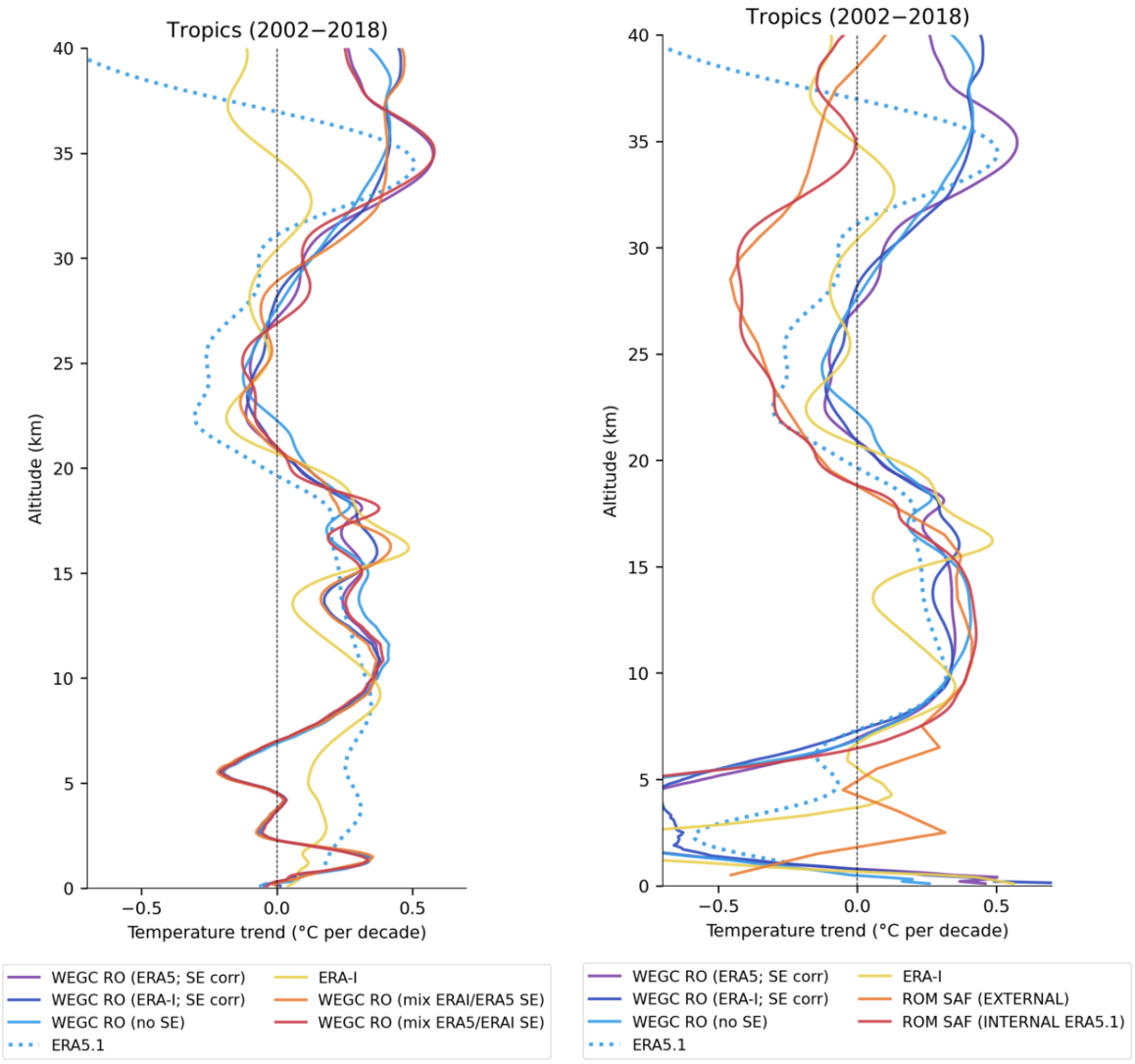

Figure 4.2: *Temperature trends from WEGC RO, without SE correction and corrected using ERA-Interim and ERA5.1. (Left) "mix ERAI/ERA5 SE" indicates the WEGC RO dataset which uses ERA-Interim for its first half and ERA5.1 for the second half of SE correction. For "mix ERA5/ERAI SE" it is the other way round. (Right) Including ROM SAF data in the comparison. "External" are dry temperature trend values computed at ROM SAF (with slightly different anomaly reference period than the other datasets and using mostly ERA-Interim as reference); "Internal" are temperature trends computed at WEGC with ROM SAF data, using ERA5.1 as reference.*

5 The impact of local time coverage

The Metop satellites maintain a Sun-synchronous orbit, with a equator-crossing local time of 9:30 a.m./p.m. This results in observational gaps in local time space (Figure 5.1), especially for low latitudes. Due to the limb sounding characteristics of RO, at the actual equator crossing time there are no measurements.

This limited local time coverage of Metop, together with the increasing share of Metop observations during time, raises the question of the impact of local time coverage on trend estimates. The local time component on the SE estimate for CHAMP and Metop-A has been investigated e.g. by [5].

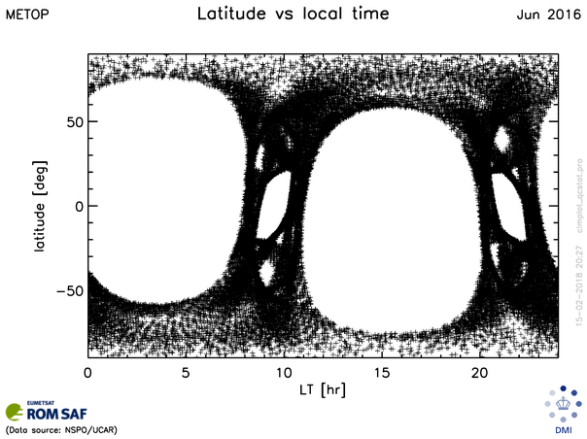

Figure 5.1: *Local time coverage of a month of observations of METOP-A/B. Figure courtesy of ROM SAF.*

The monthly local time coverage of the F3C mission is very good, and is therefore well suited to investigate local time effects. In Figure 5.2, the impact of sub-sampling F3C events to local times comparable to Metop is shown. Since the actual local time distribution of RO is blurred due to the limb sounding technique, a range of local times is chosen in the following to simulate Metop local time coverage. In Figure 5.2, the full F3C dataset is compared to one where only F3C events are selected which fall into a local time range of 9 to 10 a.m./p.m., and to one with the more realistic 8 to 11 a.m./p.m. range. The resulting trends are compared to Metop-A trends, the full F3C coverage, and to trends from all available missions.

In the tropics (Figure 5.2 left panel), the “1-hour” local time range around 9:30 differs from the complete F3C dataset above about 23 km. These datasets are all SE corrected, but the SE correction seems not to be able to correct for the missing local time coverage. Another possible reason for the bias is the very small number of events coming through the local time filter here.

For the “3-hours” local time range around 9:30, the bias to the complete F3C dataset is smaller.

The near-global trends (Figure 5.2 right panel) show comparable trends for both the “1-hour” and “3-hours” local time range. In both cases, the trends deviate from the complete F3C dataset, indicating that the SE correction possibly might not be able to account for the missing local time coverage.

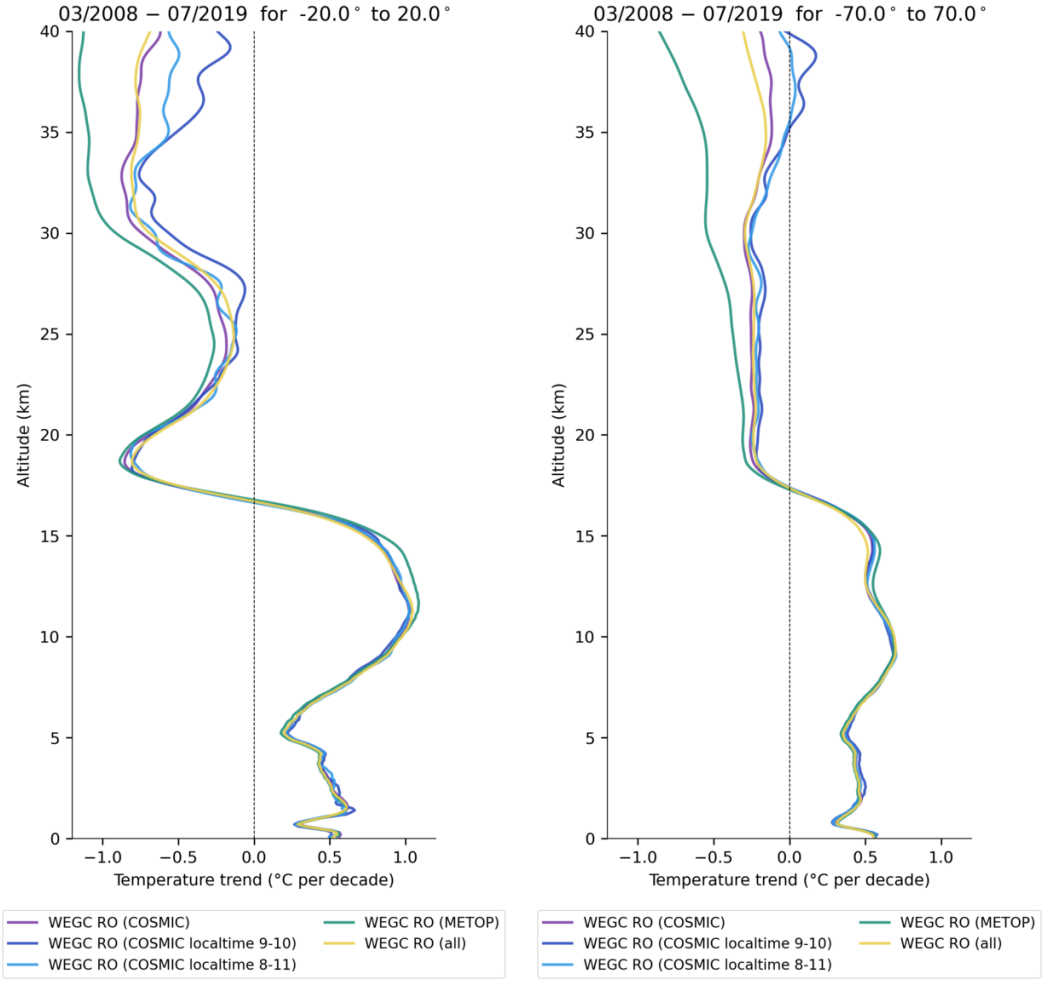

Figure 5.2: *Impact of local time coverage. "COSMIC localtime 9-10" includes only profiles within 9 and 10 a.m./p.m.; "COSMIC localtime 8-11" includes only profiles within 8 and 11 a.m./p.m.; (left) tropics, (right) near-global.*

The impact of the SE correction is shown in Figure 5.3 for the "3-hours" local time range, and in Figure 5.4 for the "1-hour" local time range. For the complete F3C dataset, the SE is close to zero below 30 km. For the "3-hours" local time range in the tropics, the temperature trend of the SE *corrected* F3C data is deviating from the complete F3C data above 30 km. Also in the global case, the SE corrected trend at altitudes above 25 km is not closer to the complete F3C trend than the non-corrected trend. Below around 25 km, the SE correction is working well.

For the "1-hour" local time range, the difference between non-corrected and SE corrected trends is larger than for the "3-hours" case, as expected. The SE correction is again not working properly for altitudes above 25 km to 30 km.

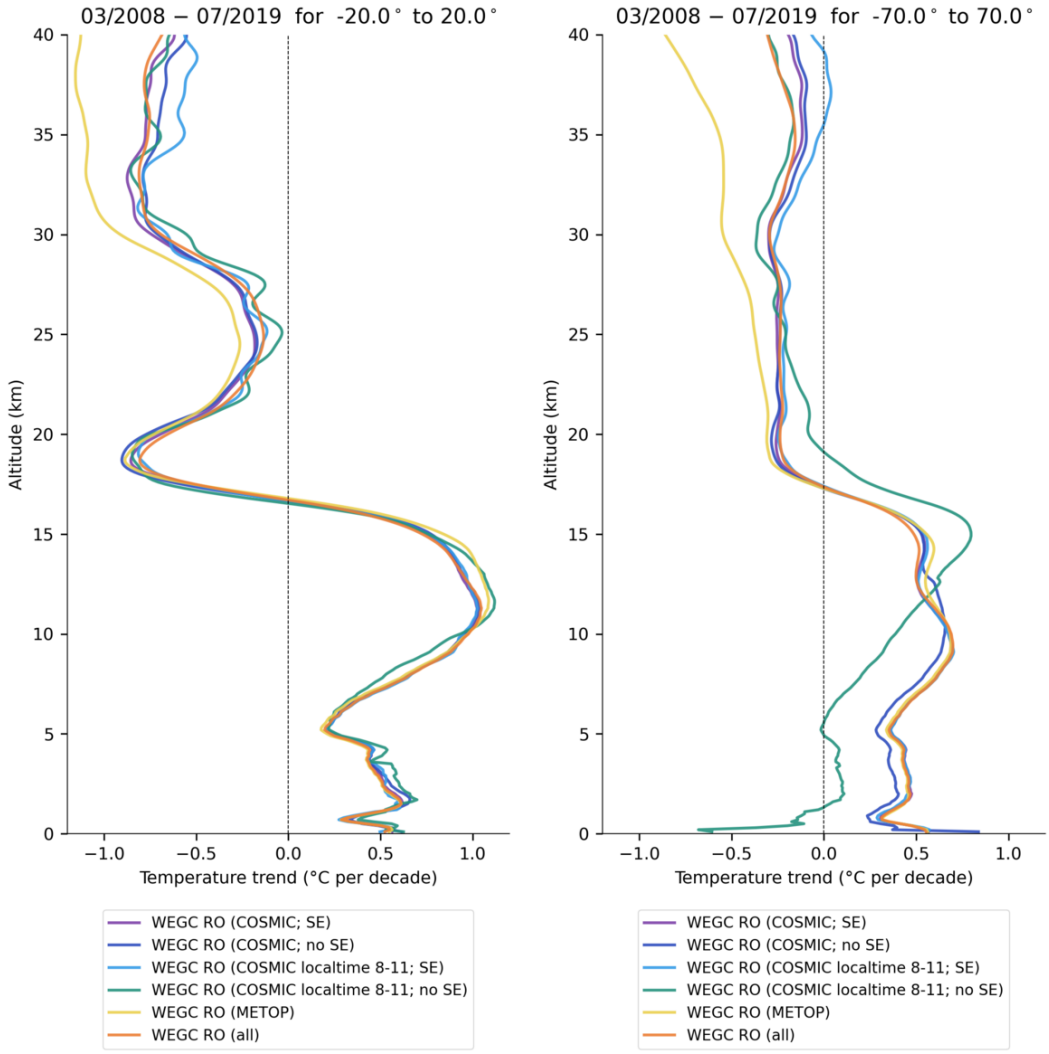

Figure 5.3: *Impact of local time coverage with and without SE correction. "COSMIC local-time 8-11" includes only profiles within 8 and 11 a.m./p.m.*

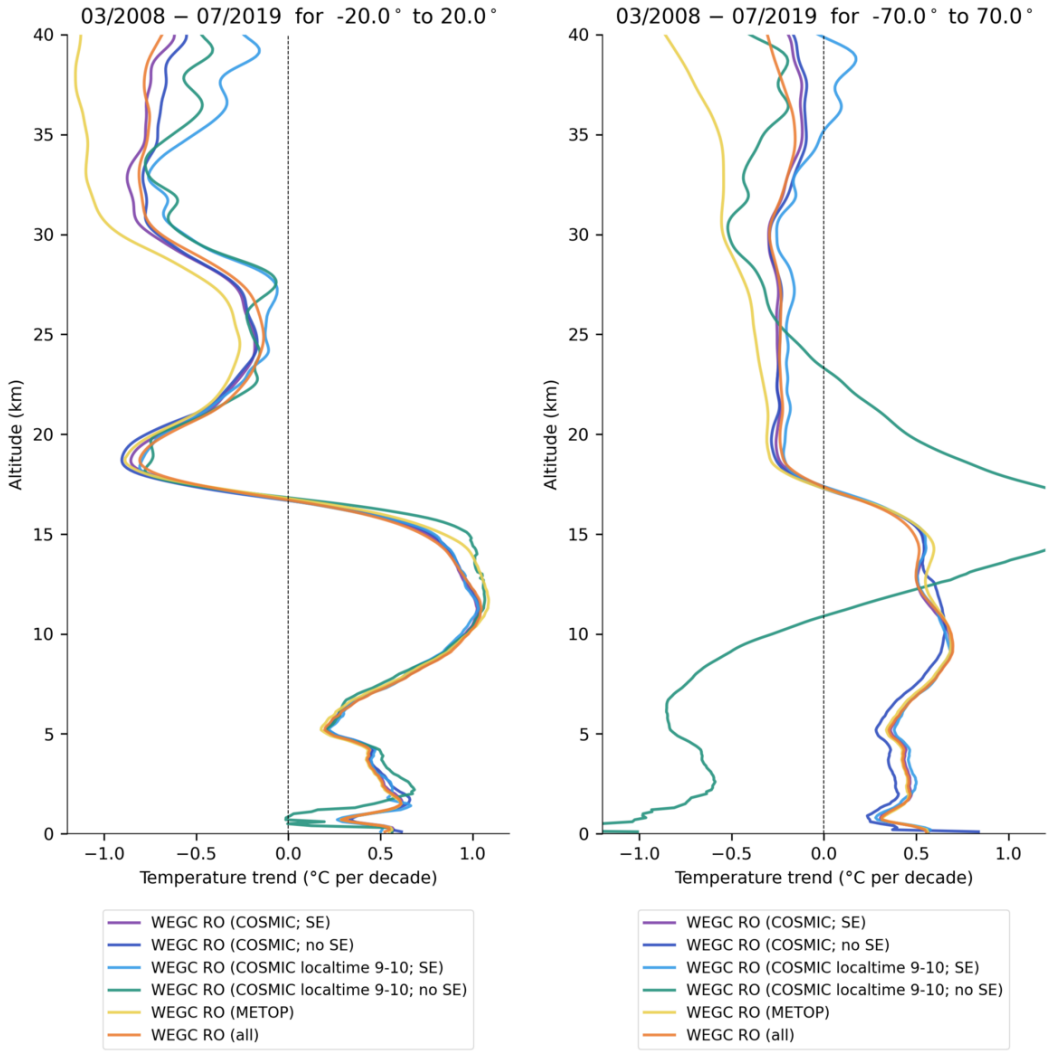

Figure 5.4: *Impact of local time coverage with and without SE correction. "COSMIC local-time 9-10" includes only profiles within 9 and 10 a.m./p.m.*

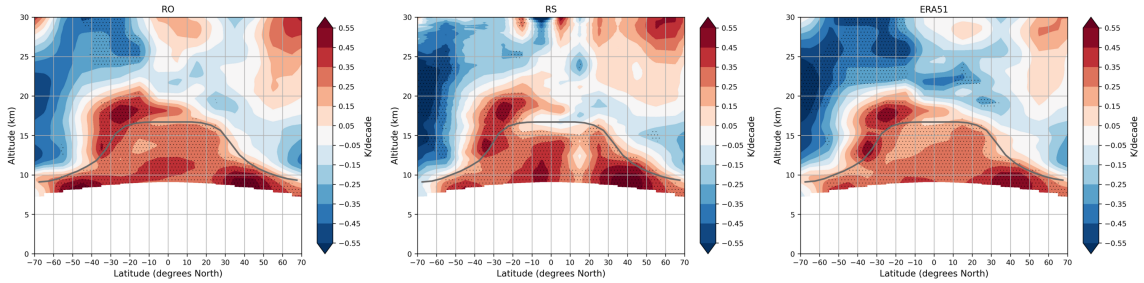

Figure 6.1: *Decadal temperature trends for 2002-01 to 2018-12 for WEGC RO (left), Vaisala radiosondes (center), and ERA5.1 (right). RO and RS are SE corrected using ERA5.1.*

6 Investigating the trend structure

This chapter takes a closer look on the details of the actual trend structure, and investigates the robustness of this structure.

6.1 Investigating the trend asymmetry at 17 km, 25 deg N/S

6.1.1 Background

The latitudinal-height resolved temperature trends from 2002 to 2018 show a distinct zonal asymmetry, with a positive blob at around 25° S/17 km, and a small negative trend at 25° N at the same height. This feature shows in RO, ERA5.1, and also in sampling-error corrected Vaisala radiosondes (Figure 6.1). Also MSU Temperature Lower Stratosphere (TLS) trends are consistent with this, see Figure 7 in [9].

Related to the IPCC contribution plot, there was a reviewer's comment about this strong positive trend feature, asking about comments and interpretations of this feature.

6.1.2 Possible contributions: Volcanic eruptions

In [10] we investigated the influence of smaller post-2000 volcanic eruptions. We concluded that there is some effect of the smaller volcanic eruptions on trend analysis for these short time periods, but it is quite small. It could still contribute to the positive trend, since in Figure 3 of [10] we see that the largest differences in trends are quite precisely in the region we see this positive blob. The differences are less than 0.2 K/decade. The main contributions to this difference is the comparatively large eruption of Calbuco in Chile, which has a temperature imprint also outside the tropics, visible for a couple of months after the eruption in April 2015.

6.1.3 Possible contribution: SH SSW in September 2002

To investigate possible outliers in the anomalies time series which could influence the linear fit, the anomalies are plotted for WEGC RO temperature at 17 km height and for the 30° to 20°S latitudinal band in Figure 6.2. There is a large negative peak in October 2002, also visible in e.g. ERA5.1 (not shown). The date of this peak suggests a relation to the strong Southern Hemisphere (SH) Sudden Stratospheric Warming (SSW) which occurred in September 2002.

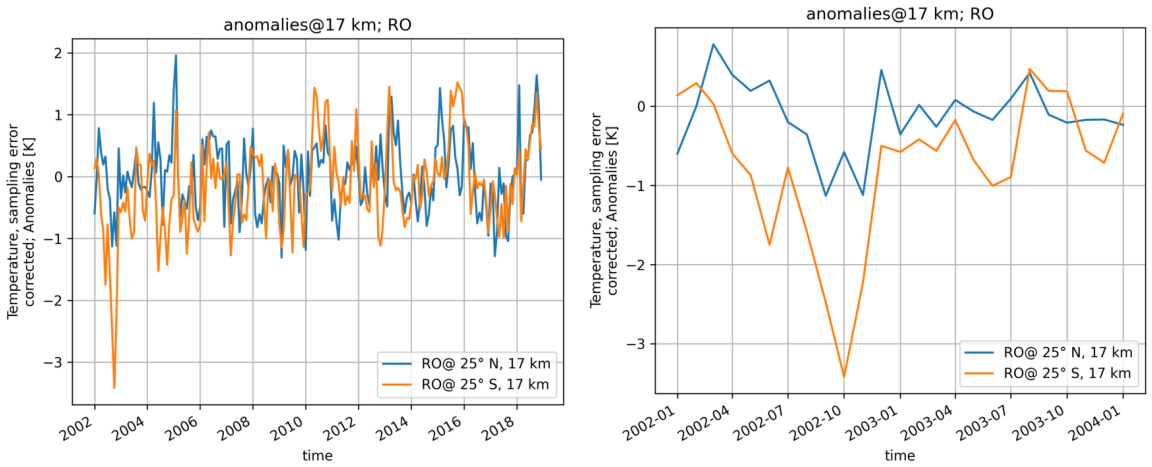

Figure 6.2: *WEGC RO temperature anomalies time series for the* 30° *to* 20°*S and* 20° *to* 30°*N latitudinal bands at* 17 km. *Full time series (left) and zoom into first two years (right).*

6.1.4 Ignoring specific months in linear fit

The influence of the 2002 SSW and of Calbuco in 2015 is investigated in Figure 6.3 by successively ignoring the months when those events impacted the atmosphere in the linear fit. Only part of the asymmetry (half?) can be explained just by these two phenomena. The overall asymmetric characteristic stays the same, and the underlying reason remains unclear (possibly related to ozone recovery).

6.1.5 Longitudinal trend characteristics at 17 km

Figure 6.4 includes ERA5.1 trends on a global 10x10 degrees map for one altitude layer at 17 km and the time span from 2002 to 2018. To estimate the impact of the 2002 SSW event and the Calbuco eruption in 2015, the corresponding months are again ignored in the linear fit for comparison (Figure 6.4 right panel). The influence of the 2002 SSW event on the SH high-latitude trends is clearly visible.

6.1.6 Adding 2019 and the strong SH SSW in 2019

In September 2019 the second SH SSW of the 21st century was observed. In updated trend plots extended to 2019, this second SSW is therefore also included. The impact of this second SSW is clearly visible in Figure 6.5. The two large positive peaks at the beginning and at the end of the time series for high southern latitudes partly cancel each other in the linear fit, leading to a much smaller trend there when including 2019. The impact on the trend peak at 25°S/17 km is also visible. The second SSW also results in a negative peak in the time series there, although not as pronounced as in 2002. It still leads partly to a cancellation of the positive trend blob there.

In summary, a linear fit is sensitive to large outliers, particularly at the beginning or end of the respective time series. Therefore, the resulting trends need to be analyzed carefully.

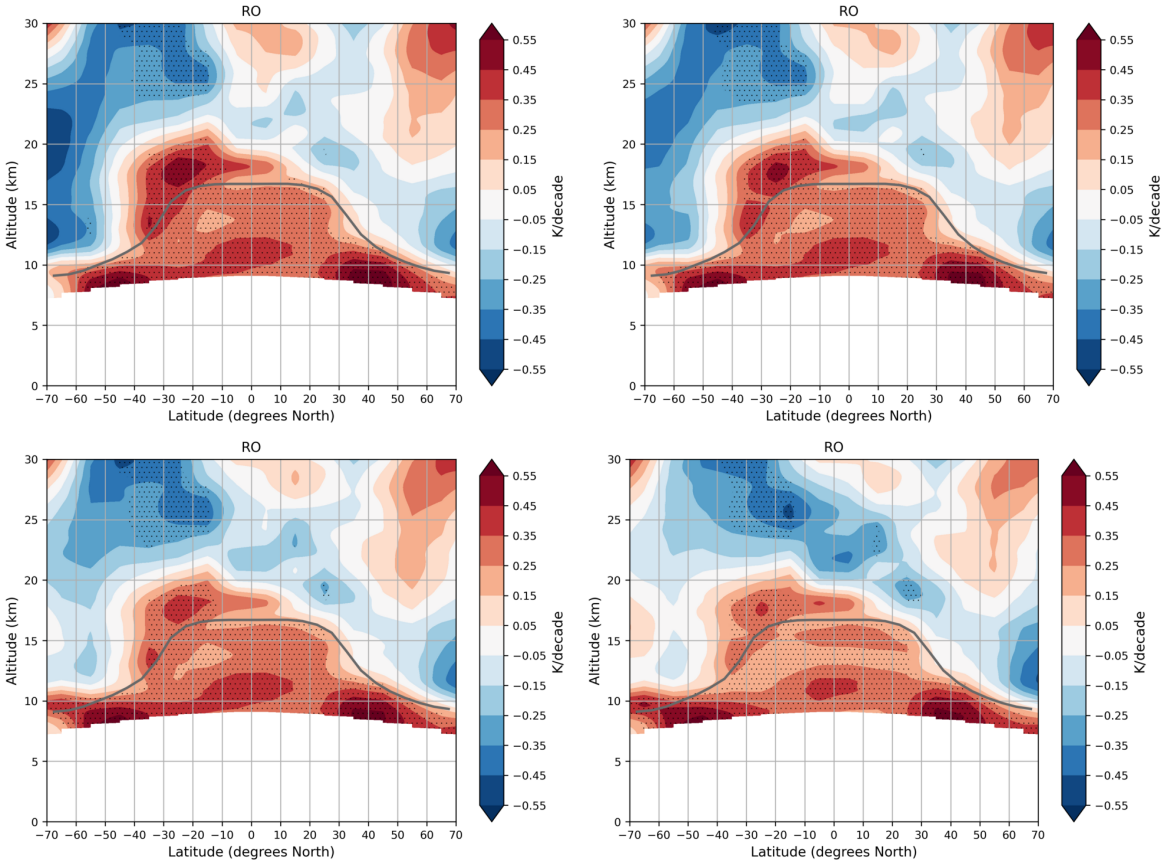

Figure 6.3: *Decadal WEGC RO temperature trends for 2002-01 to 2018-12 for the whole time series (top left), ignoring October 2002 (top right), ignoring September to November 2002 (bottom left), and ignoring both September to November 2002 and April to October 2015 (bottom right) in the linear fit.*

6.2 Multiple regression versus simple fit

In this section various multiple regression methods are compared to a simple linear fit. The statistical significance based on a 95 % level is indicated. AR(1) autocorrelation is assumed and corrected for by adjusting the standard error for the decreased degrees of freedom [7] in the case of the linear fit, and by using a Generalized Least Squares Autoregressive (GLSAR) model with AR(1) in the case of the multiple regression.

Two methods are used:

- (ENSO/QBO winds) Multiple regression based on the ENSO34 index and on the first two principle components of a Principal Component Analysis (PCA) performed on the Singapore wind profiles time series. Those indices are used over the whole latitude range. Note that this could lead to problems in the regression since El Niño–Southern Oscillation (ENSO) and Quasi-Biennial Oscillation (QBO) variability is dominant in the tropics, but not at higher latitudes.

- (M2) Multiple regression based on a PCA on the RO temperature field with a base resolution of 5x5 degrees, monthly. The PCA is performed on specific latitude ranges: 30°S to 30°N; 85°S/N to 60°S/N; 30°S/N to 60°S/N. The first principle components of

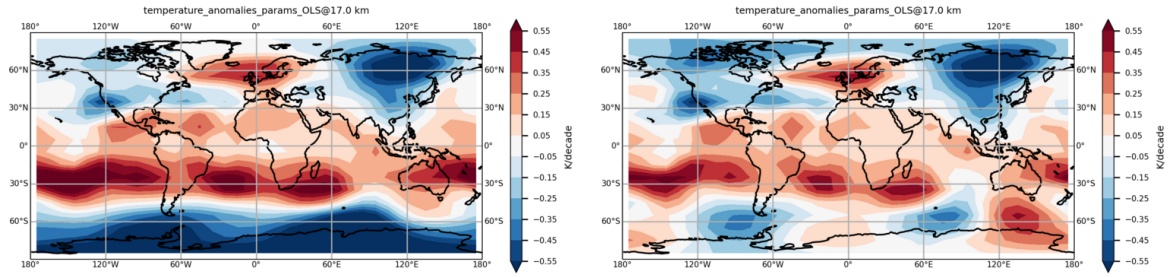

Figure 6.4: *ERA5.1 temperature trend maps for 2002-01 to 2018-12 and for* 17 km *altitude; (left) whole timeseries; (right) ignoring both 2002-09 to 2002-12 and 2015-04 to 2015-11 in the linear fit.*

each of these PCAs are then used as indices (for each altitude level separately) for the corresponding latitude ranges in the regression. See [11].

Figure 6.6 shows these two methods in comparison with a simple linear fit for WEGC RO, and to ROM SAF RO regressed with M2. The effect of the M2 regression is specifically large in the tropical stratosphere, where the strong variability caused by the QBO poses a problem to more classical approaches. In case of the linear fit, the assumption of an AR(1) behavior of the residual is certainly not fulfilled, and the estimation of the significance of trends is probably not reliable. Adding the QBO winds to the regression seems not to change much, which is probably an effect of the missing vertical resolution of the wind Principal Components (PCs). Using M2, however, results in significant trends at the 95 % level in large regions of the tropical lower to mid-stratosphere. To see the effect of the regression on the residuals, in Figure 6.7 the anomaly time series together with the corresponding residuals is depicted for an example altitude of 17 km (lowermost stratosphere). It can be seen that the M2 is very successful in removing the variability in the residuals, making the estimate of trend significance more reliable.

6.3 Remaining differences between datasets

Looking at remaining differences between the datasets in Figure 6.6, it is noticeable that trends from ROM SAF RO are more negative, especially at altitudes above 25 km and at high northern latitudes. To investigate whether this is related to general differences between the datasets (as already shown in previous chapters) or whether the atmospheric variability is covered differently by the datasets, the time series of anomalies and anomly differences are shown in Figure 6.8 for high northern lats (55° to 65°) at 30 km and 20 km altitude.

The variability is much larger (more than a factor of 2) at 30 km than at 20 km (note the different y-axis scale in the anomaly time line panels of Figure 6.8). Variability in ROM SAF RO is slightly enhanced compared to WEGC. More importantly, the anomaly differences (panel 2 and 4 in Figure 6.8) exhibit a clear trend, especially at 30 km. The anomaly differences show a distinct structure: During the CHAMP period, differences are comparatively large and positive (cf. section 2.2), and at the end of the time series the differences become negative (cf. chapter 2). Starting with 2017, ROM SAF uses only Metop data, while WEGC is still using a mixture of F3C and Metop (mostly).

In summary, the following effects are probably related to the observed differences in the

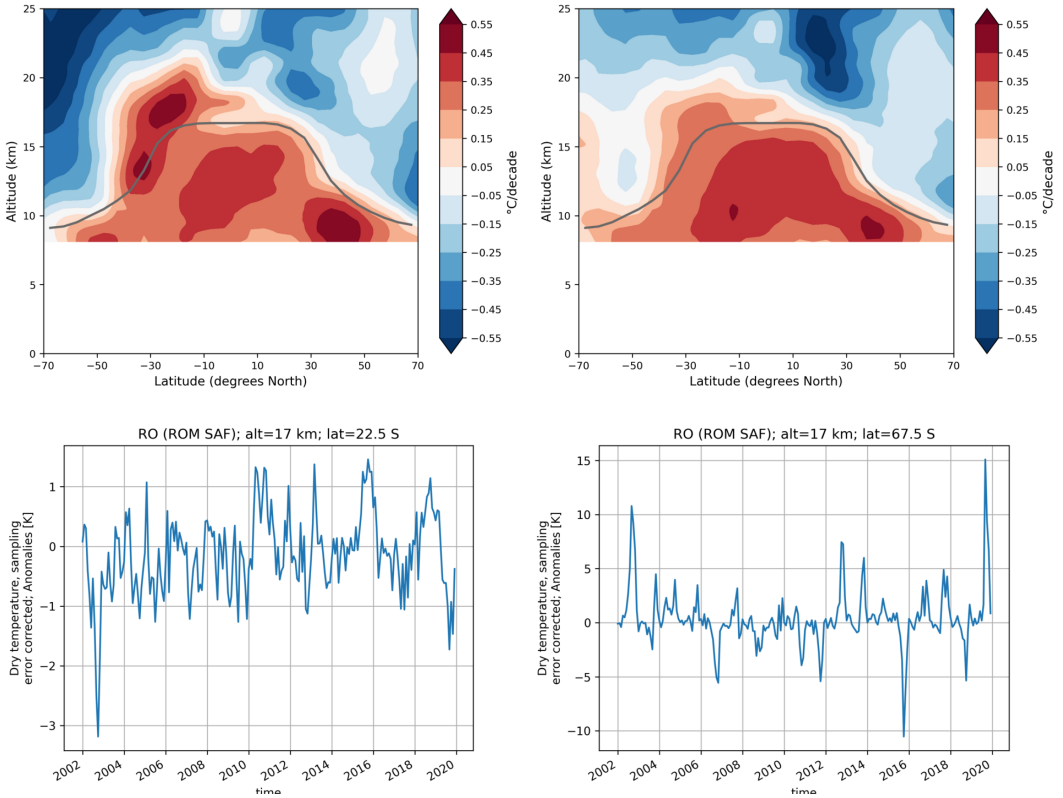

Figure 6.5: *Trends for 2002 to 2018 compared to 2002 to 2019. (top left) ROM SAF trends for 2002 to 2018, (top right) for 2002 to 2019. Trends computed at WEGC. Corresponding anomalies time series for* 17 km *height and* 20° *to* 25°*S (bottom left), and* 65° *to* 70°*S (bottom right) latitudinal bands.*

anomaly time series, and therefore the trend values:

CHAMP At higher altitudes, CHAMP compared to F3C is negatively biased for WEGC and positively biased for ROM SAF

Metop At higher altitudes, Metop trends are more negative than F3C trends for both WEGC and ROM SAF. Since ROM SAF uses only Metop after 2016, while WEGC uses a mixture of F3C and Metop, the resulting WEGC trends are slightly more positive there.

ROM SAF For ROM SAF, the positive bias at the beginning of the time series combined with giving more weight to Metop at the end of the time series, where Metop trends are more negative, results in a more negative total trend.

WEGC For WEGC, the negative bias at the beginning of the time series combined with a more positive trend at the end of the time series due to including more F3C data results in a more positive total trend.

As shown in the anomaly difference panels in Figure 6.8, multiple regression with M2 reduces the residual differences between the datasets.

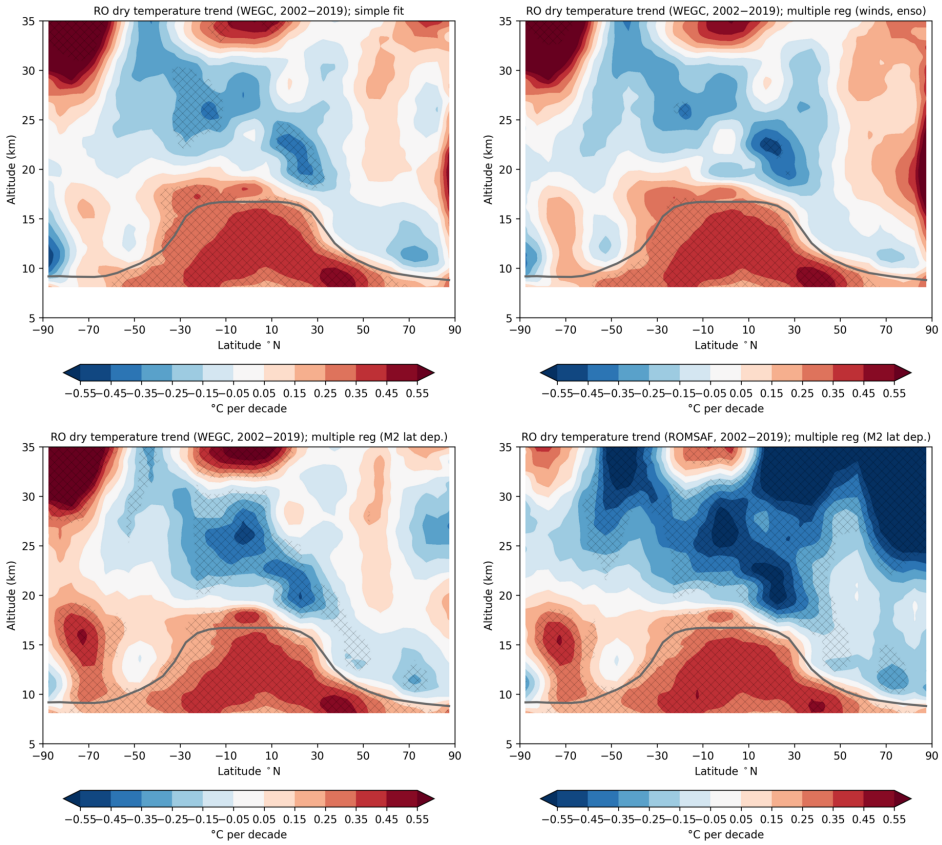

Figure 6.6: *Dry temperature trends, based on 5° latitudinal bands, SE corrected. Significant areas (95 % level) are indicated with black "X". (top left) WEGC RO, simple linear fit; (top right) WEGC RO, multiple regression, including the principle components of Singapore wind measurements, and the ENSO34 index; (bottom left) WEGC RO, multiple regression with M2, as described in the text; (bottom right) ROM SAF RO, multiple regression with M2, as described in the text.*

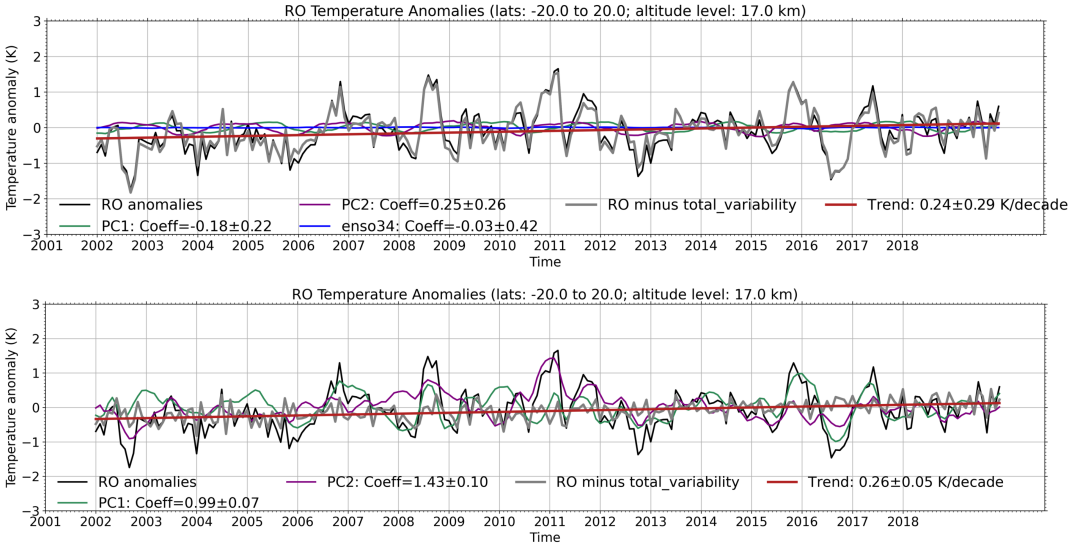

Figure 6.7: *WEGC RO temperature anomalies and regression coefficients for tropics at* 17 km. *(top) multiple regression including Singapore winds (PC1, PC2) and ENSO34 index; (bottom) multiple regression with M2 (PC1, PC2).*

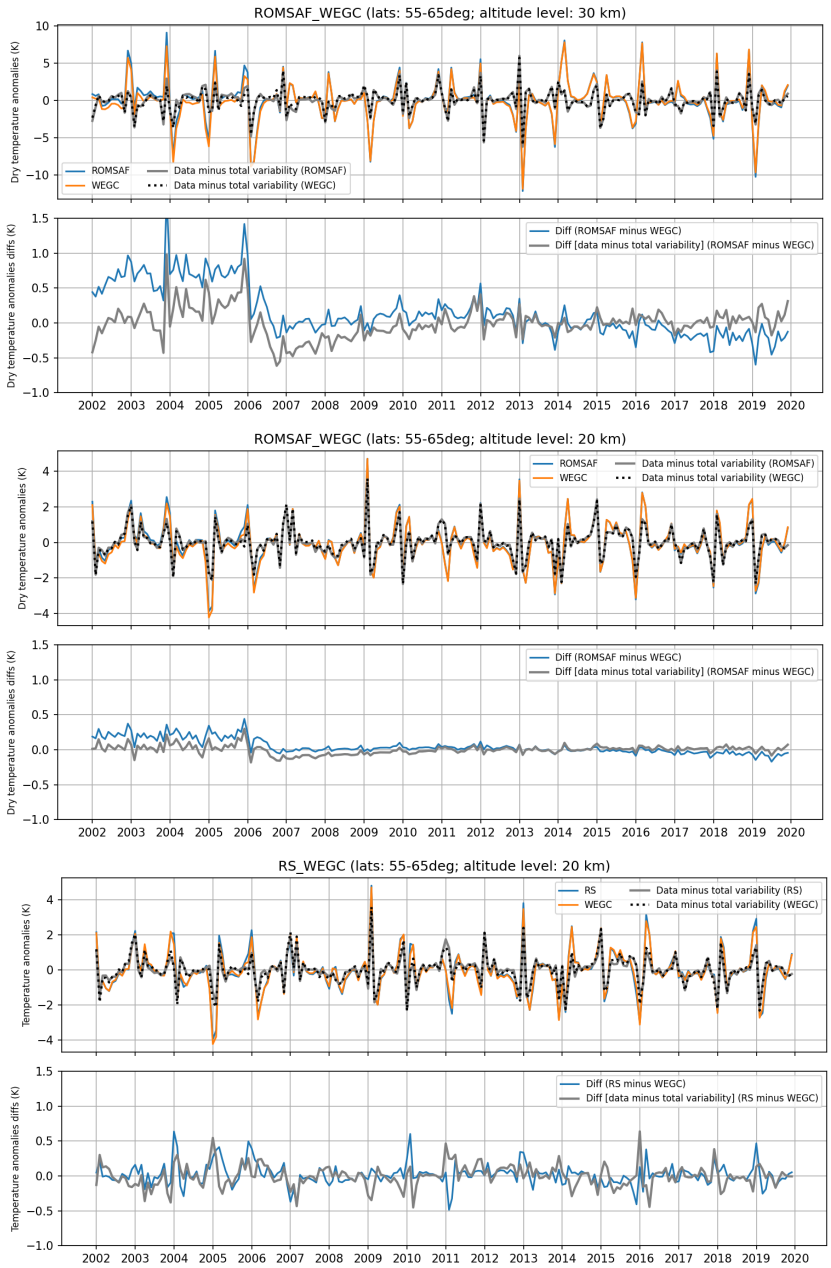

Figure 6.8: *Time series of (dry) temperature anomalies (panels 1, 3, 5) and anomaly differences (panels 2, 4, 6) at* 55° *to* 65°*N for ROM SAF and WEGC at* 30 km *(top panels), for ROM SAF and WEGC at* 20 km *(center panels), and for radiosondes and WEGC RO at* 20 km *(bottom panels). The respective top panels show the anomalies for the original data and after removing the variability with multiple regression (M2). The respective bottom panels show the differences ROM SAF minus WEGC (RS minus WEGC) between the original anomalies, and between the residual (after removing the variability). The scale for the y-axis is different for the anomaly time series plots, and the same for the anomaly difference plots.*

7 Conclusions

The contribution of the RO community to the IPCC Working Group 1 Assessment Report has triggered discussions about differences between trend estimates of RO processing centers. It has raised questions about the impacts of several choices in the data processing, trend representation, and about the quality of the presented trends. Some work has been performed to investigate various of those aspects, mainly by the team also involved in this Visiting Scientist (VS) project. This VS report should serve the purpose of consolidating the work on RO trend analysis, and to improve our understanding of the quality of climatological trends based on multi-mission RO data records. It will be accompanied by a journal publication presenting RO-based UTLS temperature trends of the 21st century.

Several factors influencing the trend estimates from RO are discussed. First, the satellite missions included in the multi-mission RO data record have an impact. Although the measurement principle of RO allows to create time series of different missions without the need of intercalibration, subtle differences can still propagate to the monthly mean data. This is of particular importance for geophysical parameters at the end of the retrieval chain. Biases between CHAMP and F3C, and between Metop and F3C are analyzed.

Second, due to the rising of levels of constant pressure with global warming, the vertical coordinate on which the measured profiles are aggregated to climatological means can influence the trend value. This is relevant when comparing trends to observations tied to pressure levels, such as radiosondes or AIRS, or when using RO data sets on pressure levels. It is an explicit advantage of RO to be able to provide measurements on an altitude grid. Care is also needed when presenting trends from measurements on altitude and pressure grids in the same figure, since the choice of mapping between altitude and pressure impacts the relative vertical position of trend values.

Third, the impact of the reference field used for SE correction on the trend values is discussed. While the choice of reference does not have a large impact on the absolute trend values, it is shown that the vertical fine structure of trends can be influenced substantially by characteristics of the reference field, especially by the one used during the CHAMP period.

Forth, both ROM SAF and WEGC multi-mission data sets are currently dominated by Metop in the last years of their respective time series. The impact of the limited local time coverage of Metop on trend values is discussed by using F3C with full and with artificially limited local time coverage as test case. Especially at higher altitudes, the effect of limited local time coverage can be non-negligible, and cannot completely be compensated by the SE correction.

And fifth, the latitudinal trend structure is analyzed, and the robustness and significance of the trends are discussed. A simple linear fit is sensitive to outliers specifically at the beginning and at the end of the time series; there, a strong natural phenomenon can influence the resulting trend value substantially. The demanding estimation of trend significance in the present of strong natural variability is also shortly discussed.

Acknowledgments

Acknowledgments go to Hans Gleisner (Danish Meteorological Institute (DMI)) for providing help through discussions and for supporting this VS, to Kent Lauritsen (DMI) and

EUMETSAT for providing me with the opportunity to work as ROM SAF Visiting Scientist, to Andrea Steiner (WEGC) for participating in discussions, and to Axel von Engeln (EUMETSAT) for coordinating the IPCC work and contributing to discussions.

Acronyms

FORMOSAT-3 Formosa Satellite mission-3.

AIRS Atmospheric Infrared Sounder.

AMSU Advanced MSU.

CHAMP Challenging Mini-Satellite Payload.

COSMIC Constellation Observing System for Meteorology, Ionosphere, and Climate.

DMI Danish Meteorological Institute.

ECMWF European Centre for Medium-Range Weather Forecasts.

ENSO El Niño–Southern Oscillation.

ERA-Interim ECMWF Re-Analysis Interim.

ERA5.1 ECMWF Re-Analysis Version 5.1.

EUMETSAT European Organization for the Exploitation of Meteorological Satellites.

F3C FORMOSAT-3/COSMIC.

FM FlightModel.

GFZ German Research Centre for Geosciences [former GeoForschungsZentrum].

GLSAR Generalized Least Squares with Autocorrelated AR(p) Errors.

GRACE Gravity Recovery and Climate Experiment.

GRIB Gridded Binary [data format].

IPCC Intergovernmental Panel on Climate Change.

JPL Jet Propulsion Laboratory.

Metop Meteorological Operational [satellite series].

Metop-A Meteorological Operational [satellite]-A.

MSU Microwave Sounding Unit.

NOAA National Oceanic and Atmospheric Administration.

PC Principal Component.

PCA Principal Component Analysis.

QBO Quasi-Biennial Oscillation.

RAOB Radiosonde Observation.

RO Radio Occultation.

ROM Radio Occultation Meteorology.

ROM SAF Radio Occultation Meteorology Satellite Application Facility.

SE Sampling Error.

SH Southern Hemisphere.

SSW Sudden Stratospheric Warming Event.

TLS Temperature Lower Stratosphere.

UCAR University Corporation for Atmospheric Research.

UG University of Graz.

UTLS Upper Troposphere–Lower Stratosphere [region].

VS Visiting Scientist [ROM SAF].

WEGC Wegener Center for Climate and Global Change [University of Graz].

Bibliography

[1] Angerer, B., Ladstädter, F., Scherllin-Pirscher, B., Schwärz, M., Steiner, A. K., Foelsche, U., and Kirchengast, G., Quality aspects of the WEGC multi-satellite GPS radio occultation record OPSv5.6, *Atmos. Meas. Tech.*, *10*, 4845–4863, 2017.

[2] Foelsche, U., Scherllin-Pirscher, B., Ladstädter, F., Steiner, A. K., and Kirchengast, G., Refractivity and temperature climate records from multiple radio occultation satellites consistent within 0.05 %, *Atmos. Meas. Tech.*, *4*, 2007–2018, 2011.

[3] Gleisner, H., Lauritsen, K. B., Nielsen, J. K., and Syndergaard, S., Evaluation of the 15-year ROM SAF monthly mean GPS radio occultation climate data record, *Atmos. Meas. Tech.*, *13*, 3081–3098, 2020.

[4] IPCC, *Climate Change 2021: The Physical Science Basis. Contribution of Working Group I to the Sixth Assessment Report of the Intergovernmental Panel on Climate Change*, Cambridge University Press, Cambridge, United Kingdom and New York, NY, USA, in press, 2021.

[5] Pirscher, B., Foelsche, U., Lackner, B. C., and Kirchengast, G., Local time influence in single-satellite radio occultation climatologies from Sun-synchronous and non-Sun-synchronous satellites, *J. Geophys. Res.*, *112*, 2007.

[6] Pirscher, B., Foelsche, U., Borsche, M., Kirchengast, G., and Kuo, Y.-H., Analysis of migrating diurnal tides detected in FORMOSAT-3/COSMIC temperature data, *J. Geophys. Res.*, *115*, 2010.

[7] Santer, B. D., Wigley, T. M. L., Boyle, J. S., Gaffen, D. J., Hnilo, J. J., Nychka, D., Parker, D. E., and Taylor, K. E., Statistical significance of trends and trend differences in layer-average atmospheric temperature time series, *J. Geophys. Res.*, *106*, 7337–7356, 2000.

[8] Steiner, A. K., Ladstädter, F., Ao, C. O., Gleisner, H., Ho, S.-P., Hunt, D., Schmidt, T., Foelsche, U., Kirchengast, G., Kuo, Y.-H., Lauritsen, K. B., Mannucci, A. J., Nielsen, J. K., Schreiner, W., Schwärz, M., Sokolovskiy, S., Syndergaard, S., and Wickert, J., Consistency and structural uncertainty of multi-mission GPS radio occultation records, *Atmos. Meas. Tech.*, *13*, 2547–2575, 2020.

[9] Steiner, A. K., Ladstädter, F., Randel, W. J., Maycock, A. C., Fu, Q., Claud, C., Gleisner, H., Haimberger, L., Ho, S.-P., Keckhut, P., Leblanc, T., Mears, C., Polvani, L. M., Santer, B. D., Schmidt, T., Sofieva, V. F., Wing, R., and Zou, C.-Z., Observed Temperature Changes in the Troposphere and Stratosphere from 1979 to 2018, *J. Climate*, *33*, 8165–8194, 2020.

[10] Stocker, M., Ladstädter, F., Wilhelmsen, H., and Steiner, A. K., Quantifying Stratospheric Temperature Signals and Climate Imprints From Post-2000 Volcanic Eruptions, *Geophys. Res. Lett.*, *46*, 12 486–12 494, 2019.

[11] Wilhelmsen, H., Ladstädter, F., Scherllin-Pirscher, B., and Steiner, A. K., Atmospheric QBO and ENSO indices with high vertical resolution from GNSS radio

occultation temperature measurements, *Atmos. Meas. Tech.*, *11*, 1333–1346, 2018.